Supporting Information

Fragment-based approach for the efficient calculation of the refractive index of metal-organic frameworks

Marvin Treger[1,3], Carolin König[2,3], Peter Behrens[1,3] and Andreas M. Schneider[1,3]

[1]Institute of Inorganic Chemistry, Leibniz University Hannover, Callinstr. 9, 30167 Hannover, Germany
[2]Institute of Physical Chemistry, Leibniz University Hannover, Callinstr. 3A, 30167 Hannover, Germany
[3]Cluster of Excellence PhoenixD (Photonics, Optics, and Engineering – Innovation Across Disciplines), Hannover, Germany

Table of Contents

Section 1 Plane wave basis set convergence and XC functional benchmark 3
UiO-66-F_4 3
UiO-67 4
Zr-fum MOF 5
MIL-140A 6
MIL-140A-F 7
MIL-140A-Cl 8
MIL-140A-Br 9
MIL-140A-NO_2 10
ZIF-8 11
ZIF-318 12
ZIF-90 13
SOD-ZIF-71 14
SALEM-2 15
ZIF-1 16
ZIF-10 17
ZIF-64 18
ZIF-72 19
Al-MIL-53 (ht) 20
Section 2 Details of the periodic DFT models 21
Section 3 Details of the molecular DFT calculations 22
Section 4 XC functional benchmark for fragment approach 23
Section 5 Polarizabilities of the MOF fragments 24
Section 6 Fragment approach example calculation 25
ZIF-8 25

UiO-66 25
Section 7 Comparison of the calculation times 26
Section 8 Band structures 28
Zr-fum MOF 28
UiO-66-F_4 29
UiO-67 29
MIL-140A 30
MIL-140A-F 30
MIL-140A-Cl 31
MIL-140A-Br 31
MIL-140A-NO_2 32
ZIF-8 32
ZIF-318 33
ZIF-90 33
SOD-ZIF-71 34
SALEM-2 34
ZIF-1 35
ZIF-10 35
ZIF-64 36
ZIF-72 36
Al-MIL-53 (ht) 37
Section 9 Dispersion of the refractive indices 38
UiO-66 type MOFs 38
MIL-140A and derivatives 39
ZIF-8 and derivatives 39
ZIFs with im linker 40
ZIF-72 40
Al-MIL-53 41
Section 10 Comparison of the calculated refractive indices 42
References 46

Section 1 Plane wave basis set convergence and XC functional benchmark

The kinetic plane wave energy cutoff convergence was tested with respect to the lattice parameters of the primitive cells and the threshold was set to a change of 0.01 Å. The sampling of the Brillouin zone was tested with respect to the total energy and the lattice parameters of the primitive cells.

UiO-66-F$_4$

The sampling of the Brillouin zone of UiO-66 type MOFs was tested with respect to the total energy and the lattice parameters of the primitive cells in our previous work. [1] [2]

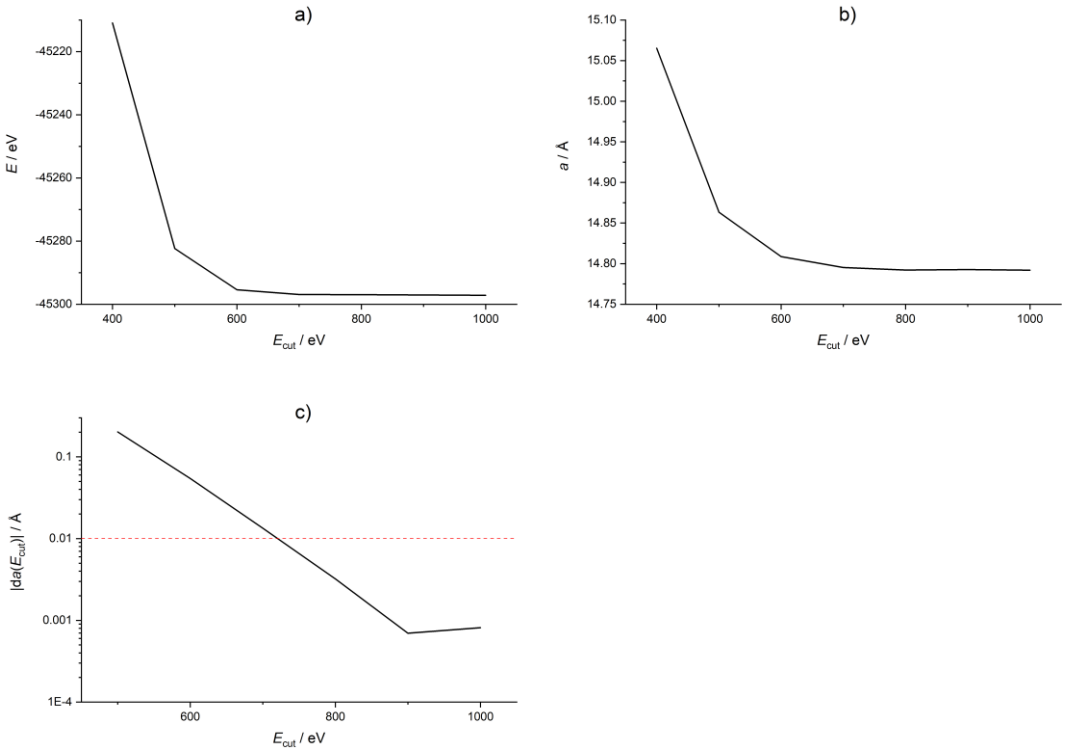

Figure S1. UiO-66-F$_4$: Convergence of a) total energy, b) lattice parameter *a* and c) lattice parameter *a* (derivation).

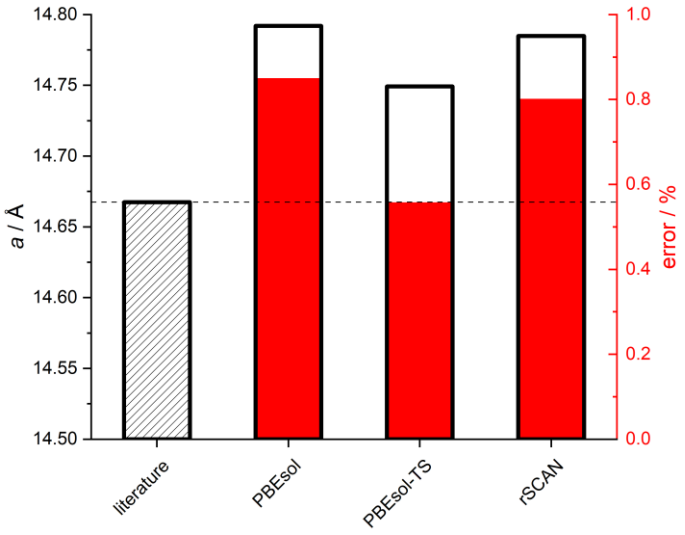

Figure S2. UiO-66-F$_4$: XC functional benchmark (absolute value black with relative error in red). Literature value taken from Reference [3].

UiO-67

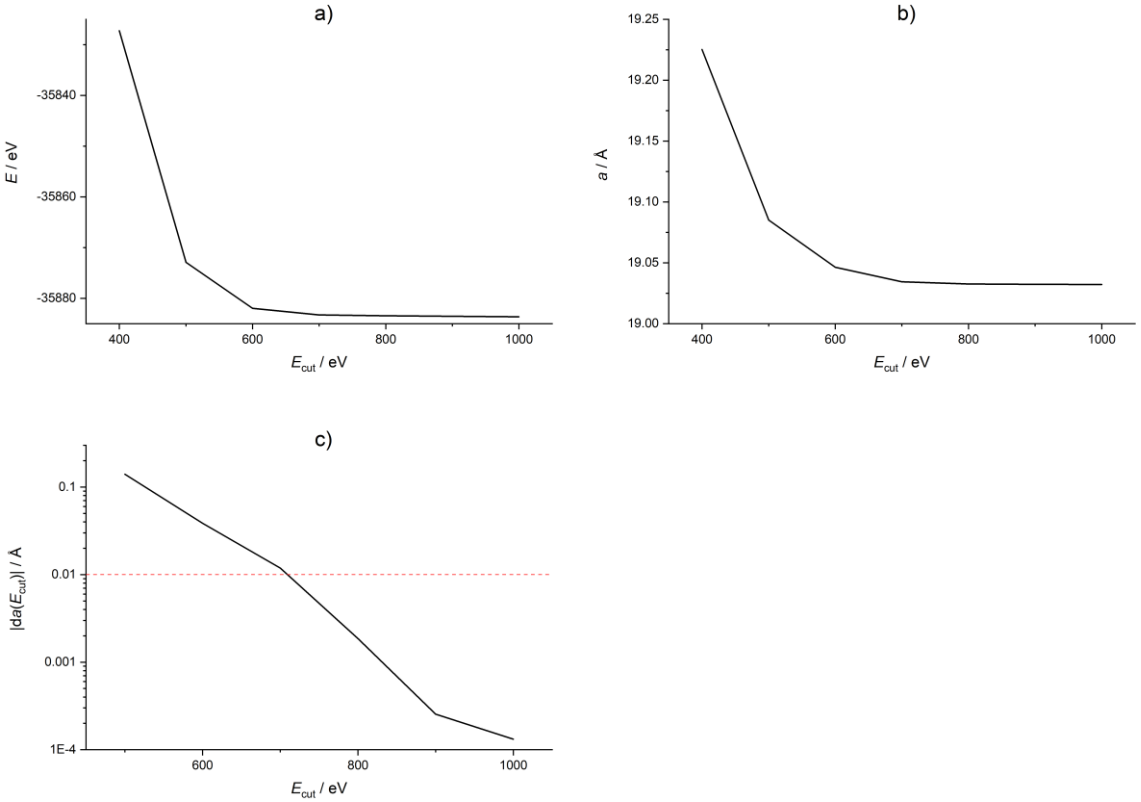

Figure S3. UiO-67: Convergence of a) total energy, b) lattice parameter *a* and c) lattice parameter *a* (derivation).

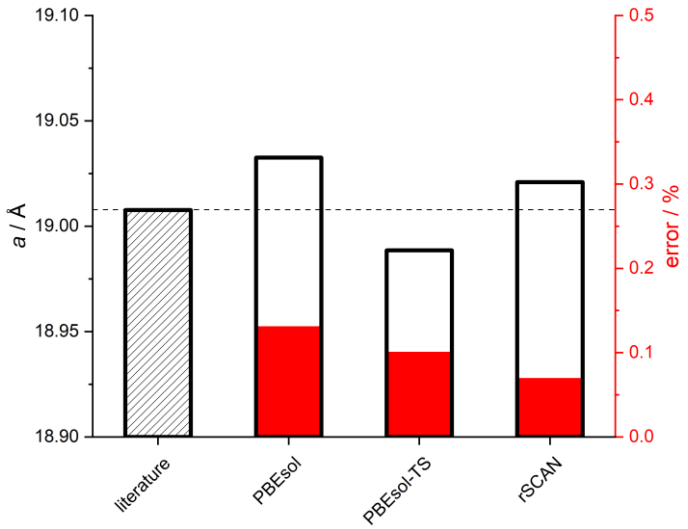

Figure S4. UiO-67: XC functional benchmark (absolute value black with relative error in red). Literature value taken from Reference [3].

Zr-fum MOF

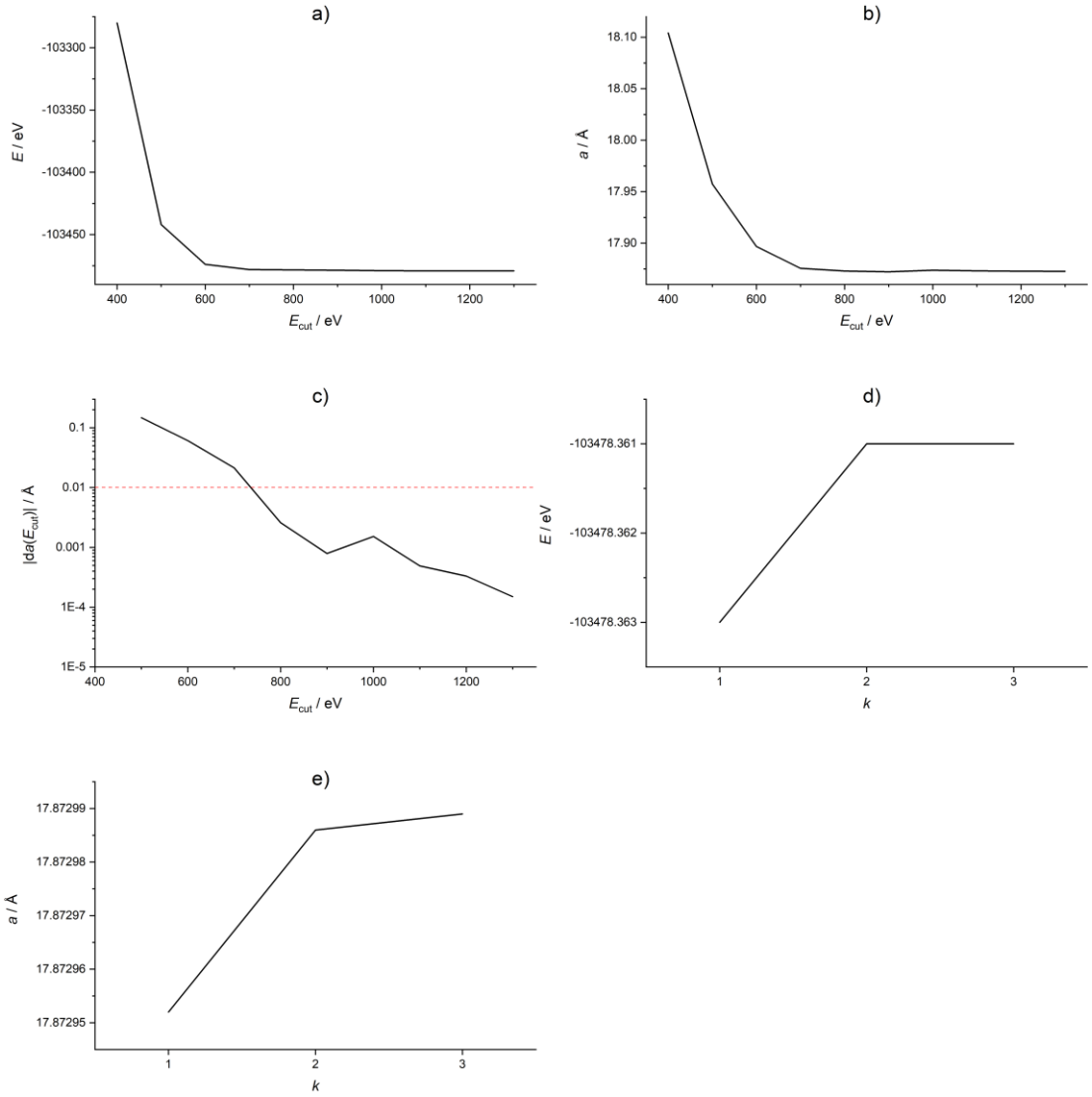

Figure S5. Zr-*fum* MOF: Convergence of a) total energy, b) lattice parameter *a*, c) lattice parameter *a* (derivation), d) k points (energy) and e) k points (lattice).

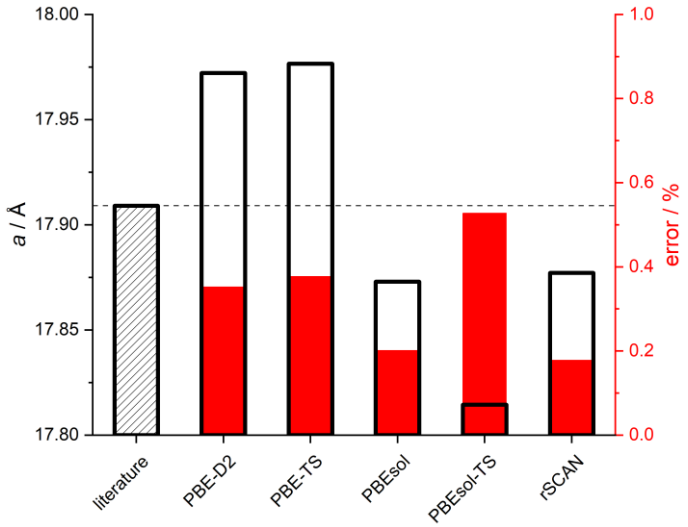

Figure S6. Zr-*fum* MOF: XC functional benchmark (absolute value black with relative error in red). Literature value taken from Reference [4].

MIL-140A

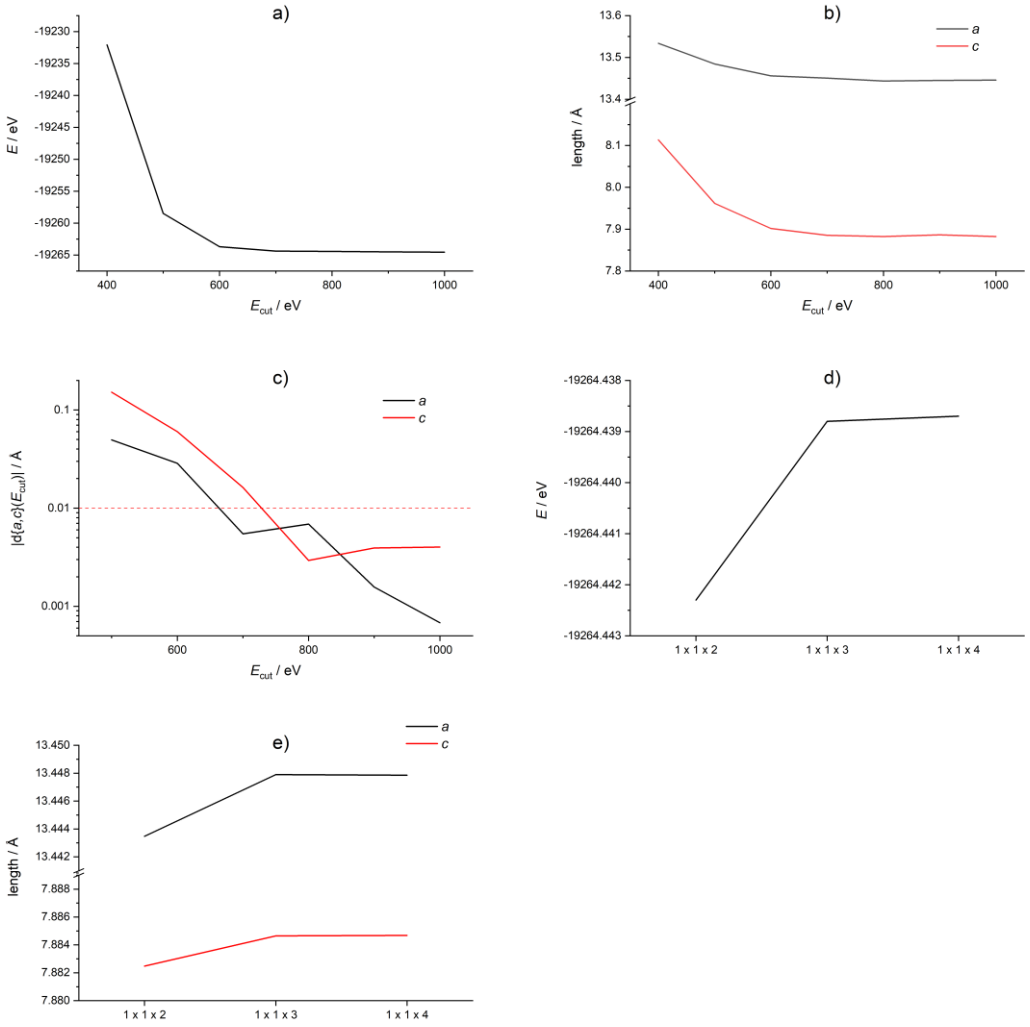

Figure S7. MIL-140A: Convergence of a) total energy, b) lattice parameter *a* and c, and c) lattice parameter *a* and c (derivation), d) k points (energy) and e) k points (lattice).

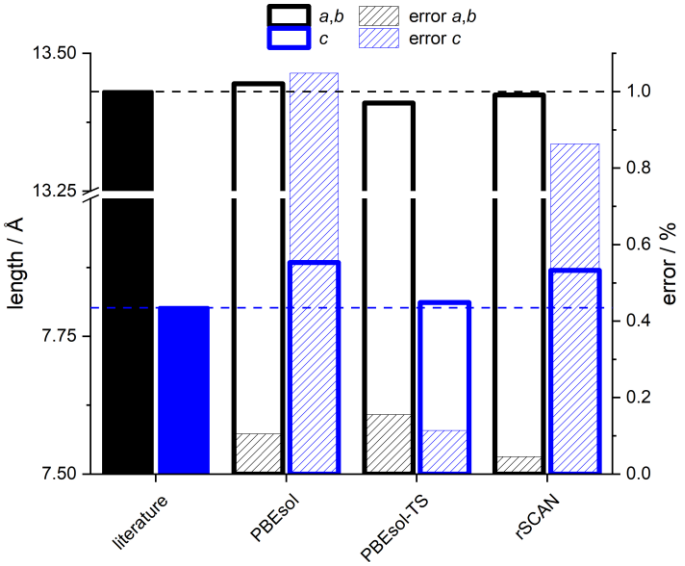

Figure S8. MIL-140A: XC functional benchmark with lattice parameters *a*, *b* and *c* (absolute values solid with relative errors hatched). Literature value taken from Reference [5].

MIL-140A-F

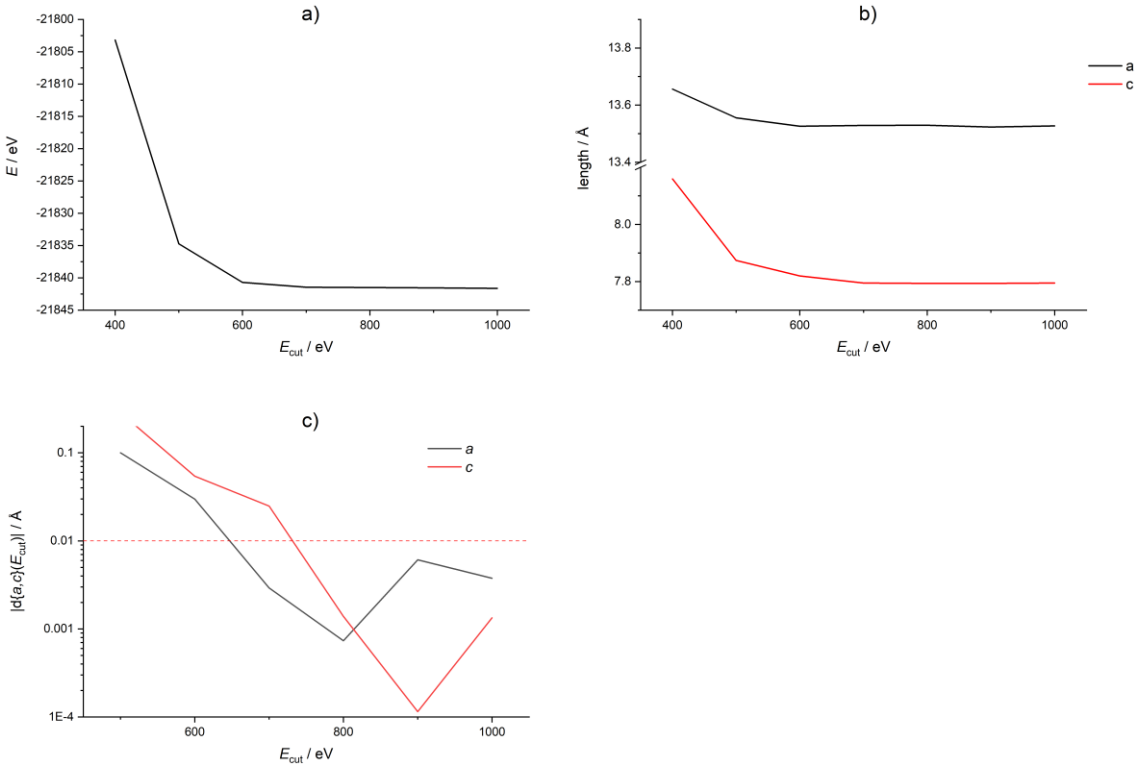

Figure S9. MIL-140A-F: Convergence of a) total energy, b) lattice parameter *a* and c, and c) lattice parameter *a* and c (derivation).

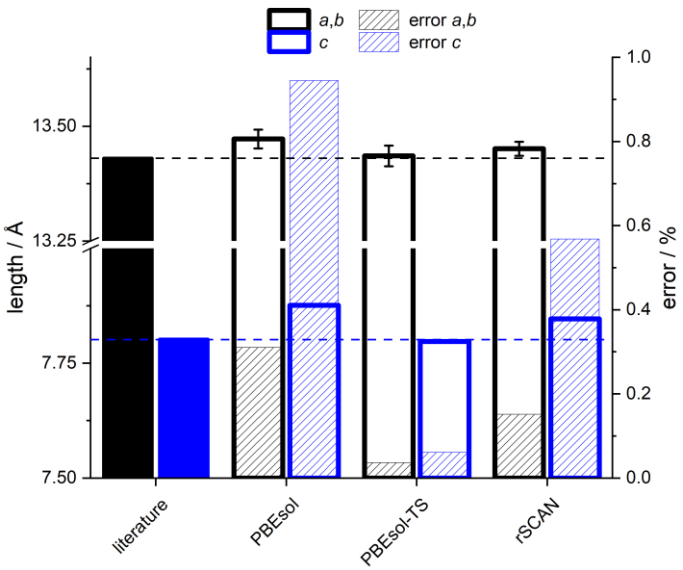

Figure S10. MIL-140A-F: XC functional benchmark with average of lattice parameters *a* and *b* and lattice parameter *c* (absolute values solid with relative errors hatched). Literature value taken from Reference [5].

MIL-140A-Cl

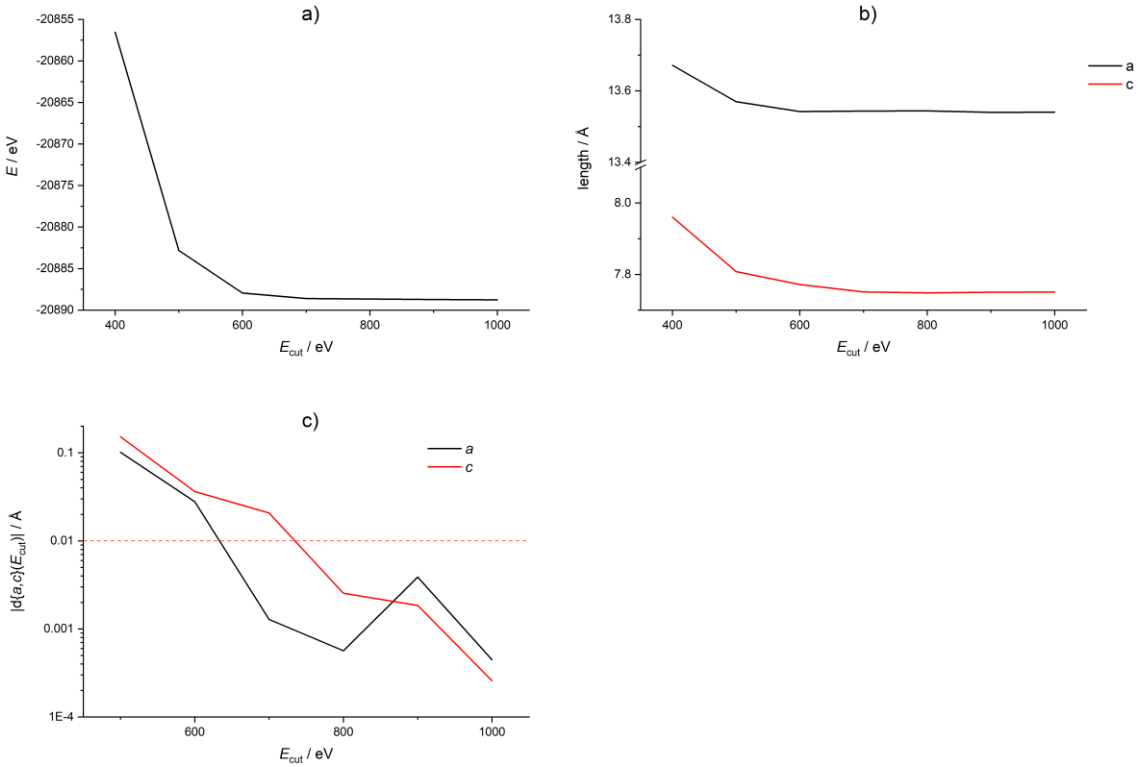

Figure S11. MIL-140A-Cl: Convergence of a) total energy, b) lattice parameter *a* and c, and c) lattice parameter *a* and c (derivation).

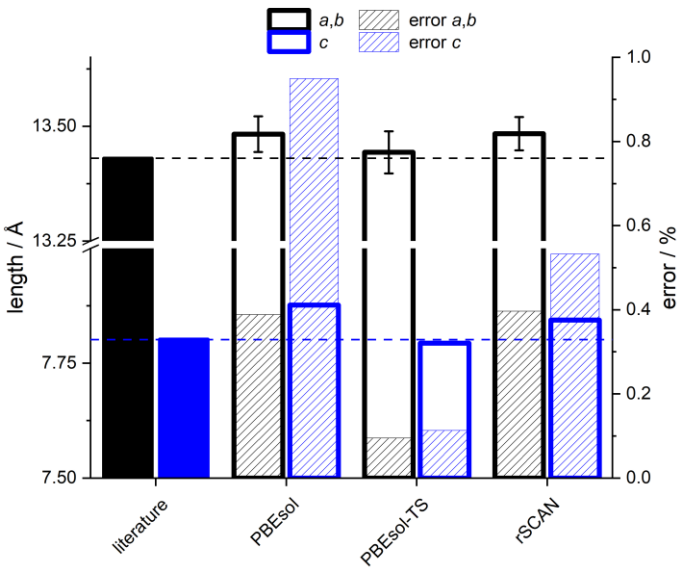

Figure S12. MIL-140A-Cl: XC functional benchmark with average of lattice parameters *a* and *b* and lattice parameter *c* (absolute values solid with relative errors hatched). Literature value taken from Reference [5].

MIL-140A-Br

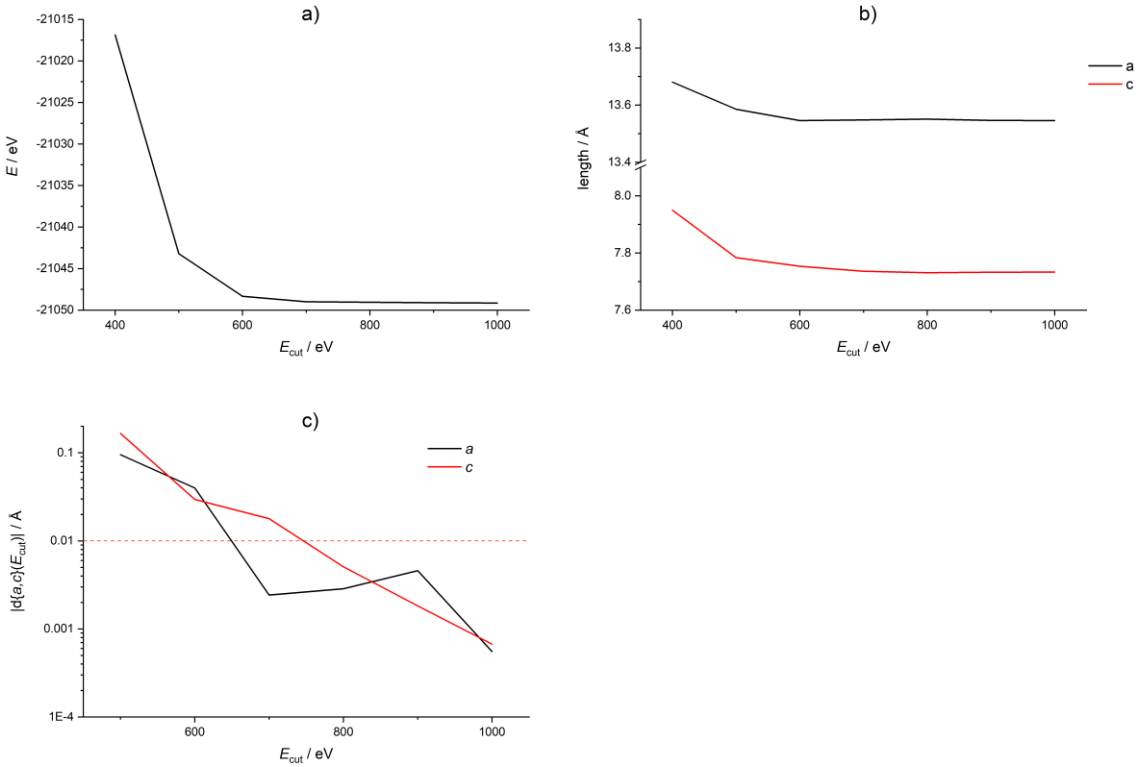

Figure S13. MIL-140A-Br: Convergence of a) total energy, b) lattice parameter *a* and c, and c) lattice parameter *a* and c (derivation).

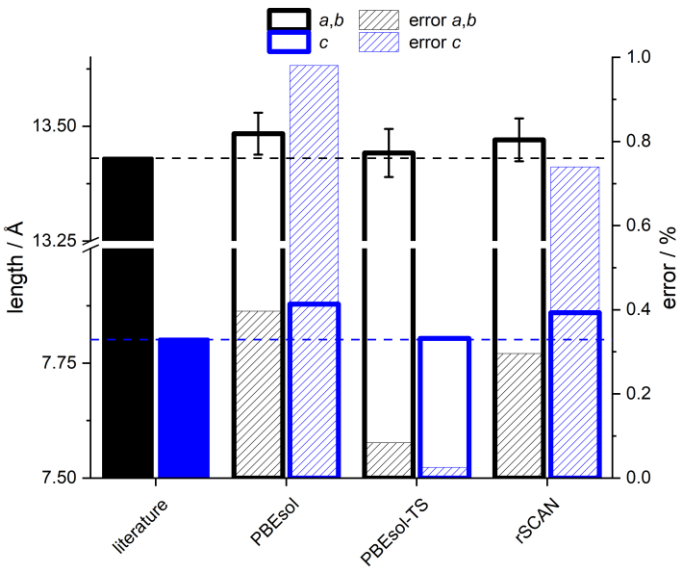

Figure S14. MIL-140A-Br: XC functional benchmark with average of lattice parameters *a* and *b* and lattice parameter *c* (absolute values solid with relative errors hatched). Literature value taken from Reference [5].

MIL-140A-NO_2

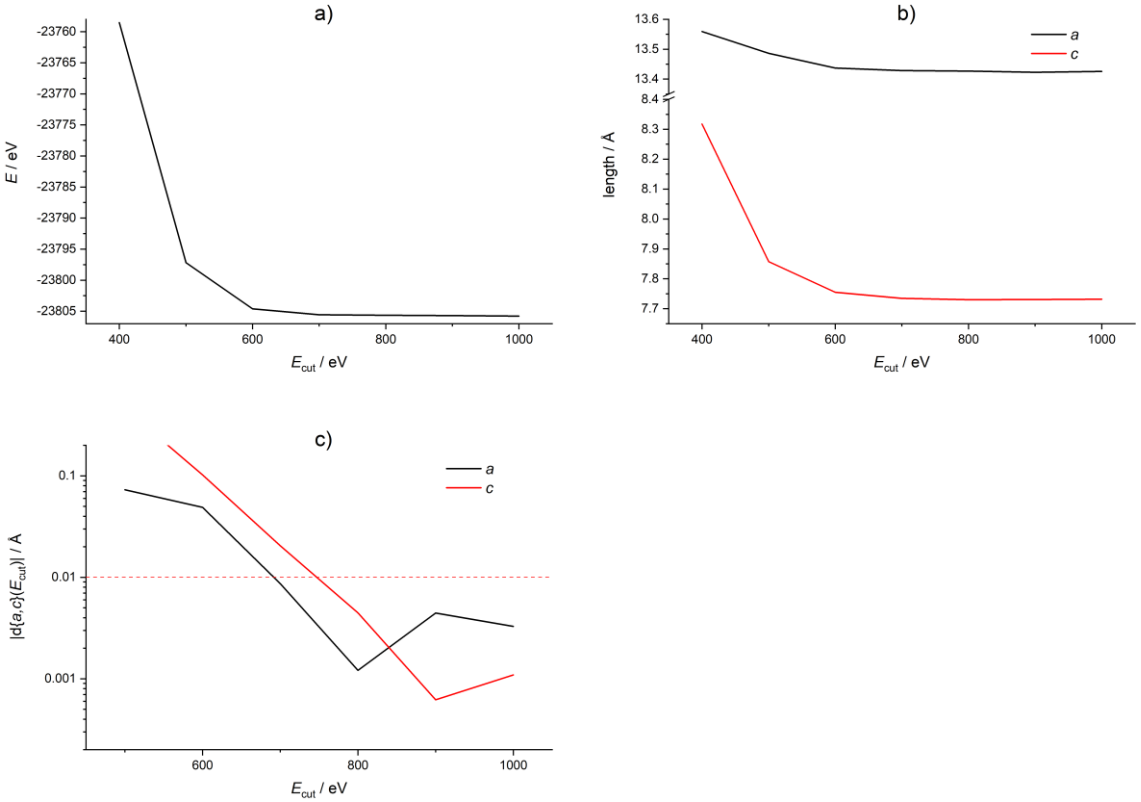

Figure S15. MIL-140A-NO_2: Convergence of a) total energy, b) lattice parameter *a* and c, and c) lattice parameter *a* and c (derivation).

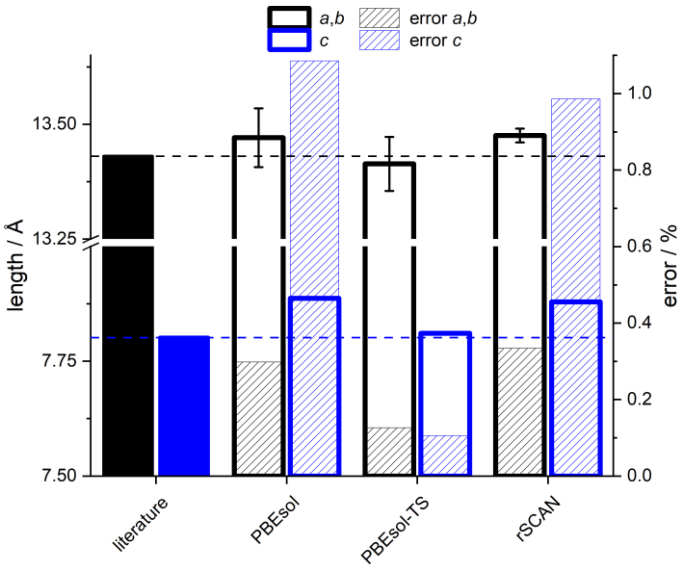

Figure S16. MIL-140A-NO_2: XC functional benchmark with average of lattice parameters *a* and *b* and lattice parameter *c* (absolute values solid with relative errors hatched). Literature value taken from Reference [5].

ZIF-8

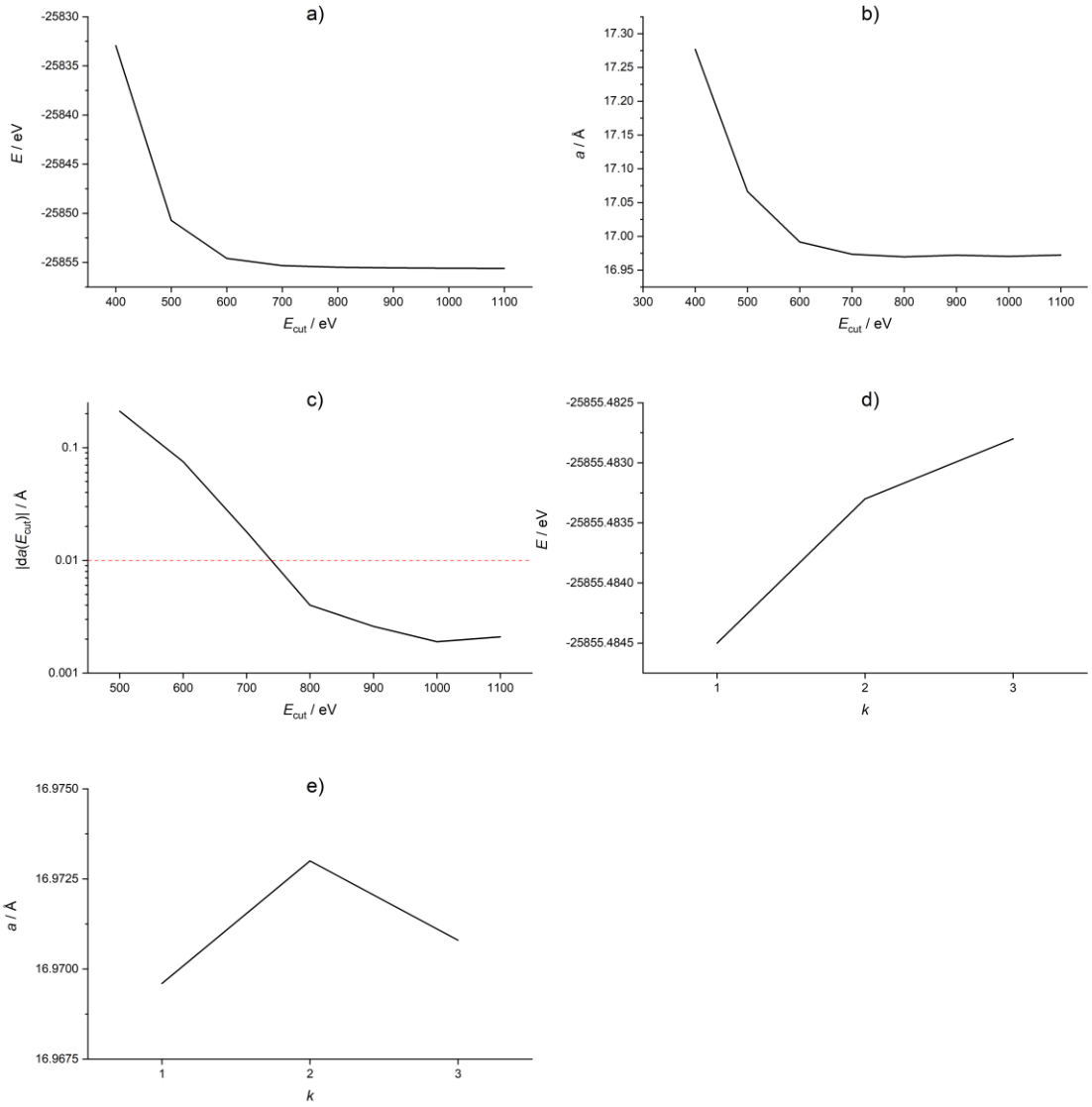

Figure S17. ZIF-8: Convergence of a) total energy, b) lattice parameter *a*, c) lattice parameter *a* (derivation), d) k points (energy) and e) k points (lattice).

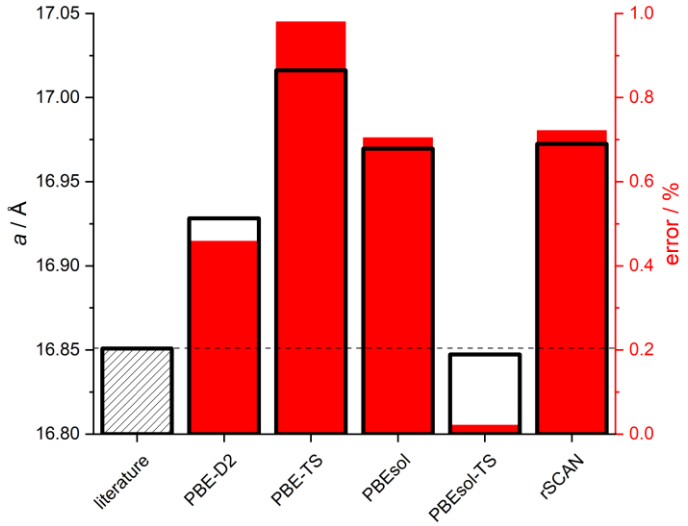

Figure S18. ZIF-8: XC functional benchmark (absolute value black with relative error in red). Literature value taken from Reference [6].

ZIF-318

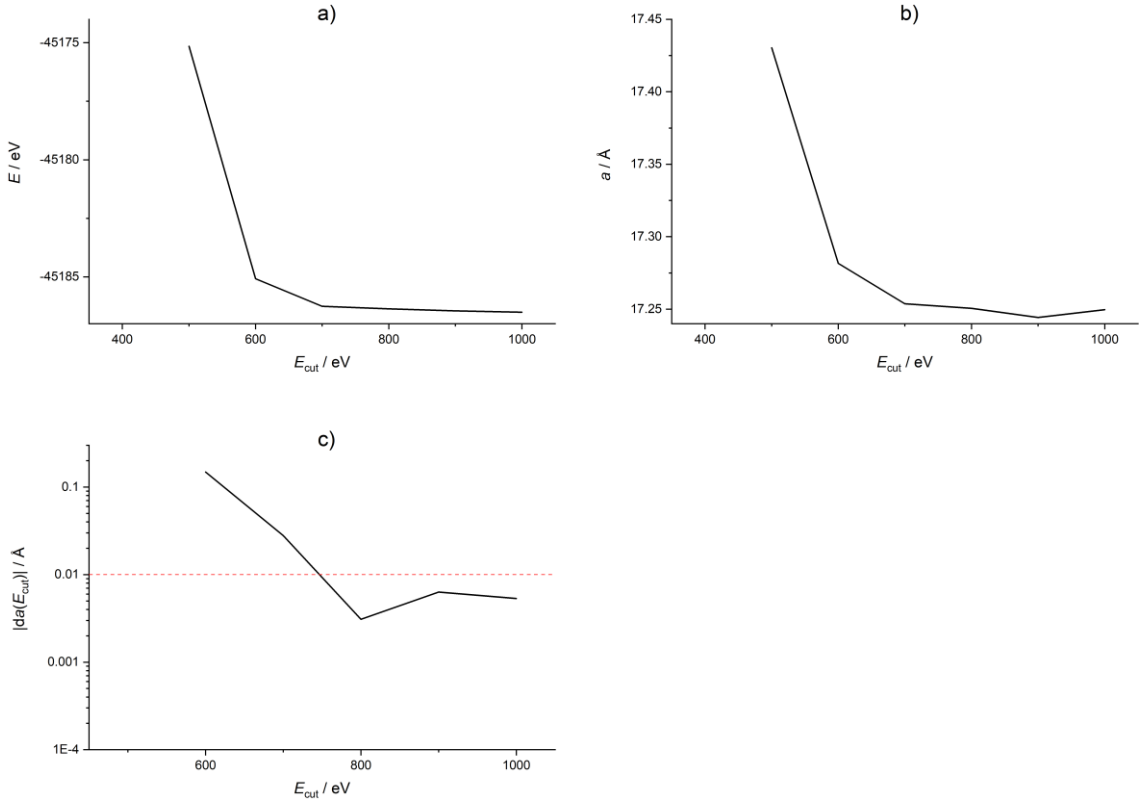

Figure S19. ZIF-318: Convergence of a) total energy, b) lattice parameter *a* and c) lattice parameter *a* (derivation).

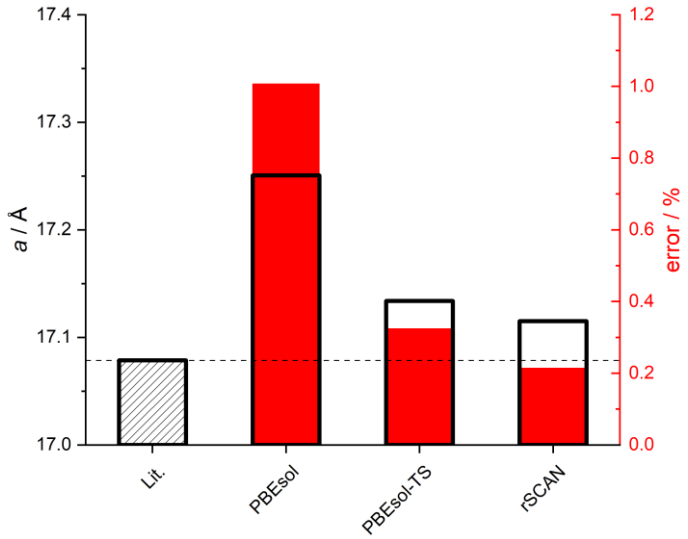

Figure S20. ZIF-318: XC functional benchmark (absolute value black with relative error in red). Literature value taken from Reference [7].

ZIF-90

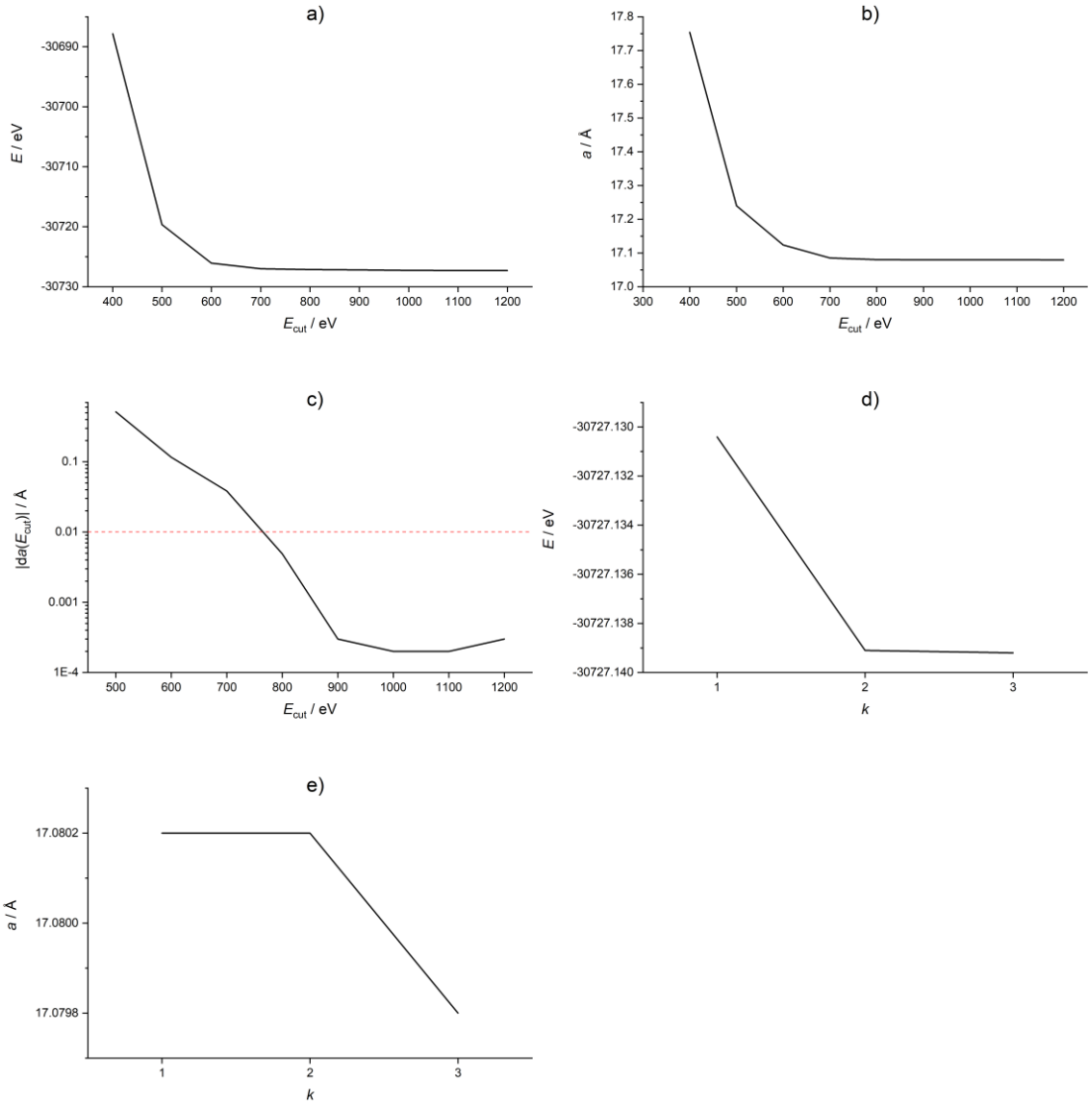

Figure S21. ZIF-90: Convergence of a) total energy, b) lattice parameter *a*, c) lattice parameter *a* (derivation), d) k points (energy) and e) k points (lattice).

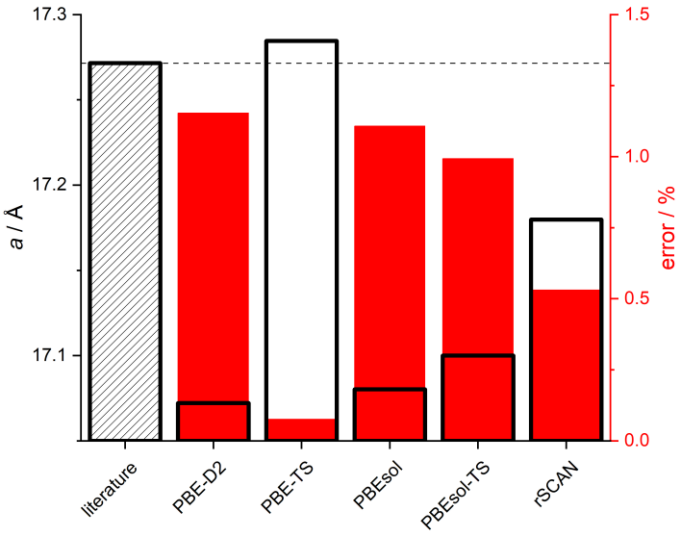

Figure S22. ZIF-90: XC functional benchmark (absolute value black with relative error in red). Literature value taken from Reference [8].

SOD-ZIF-71

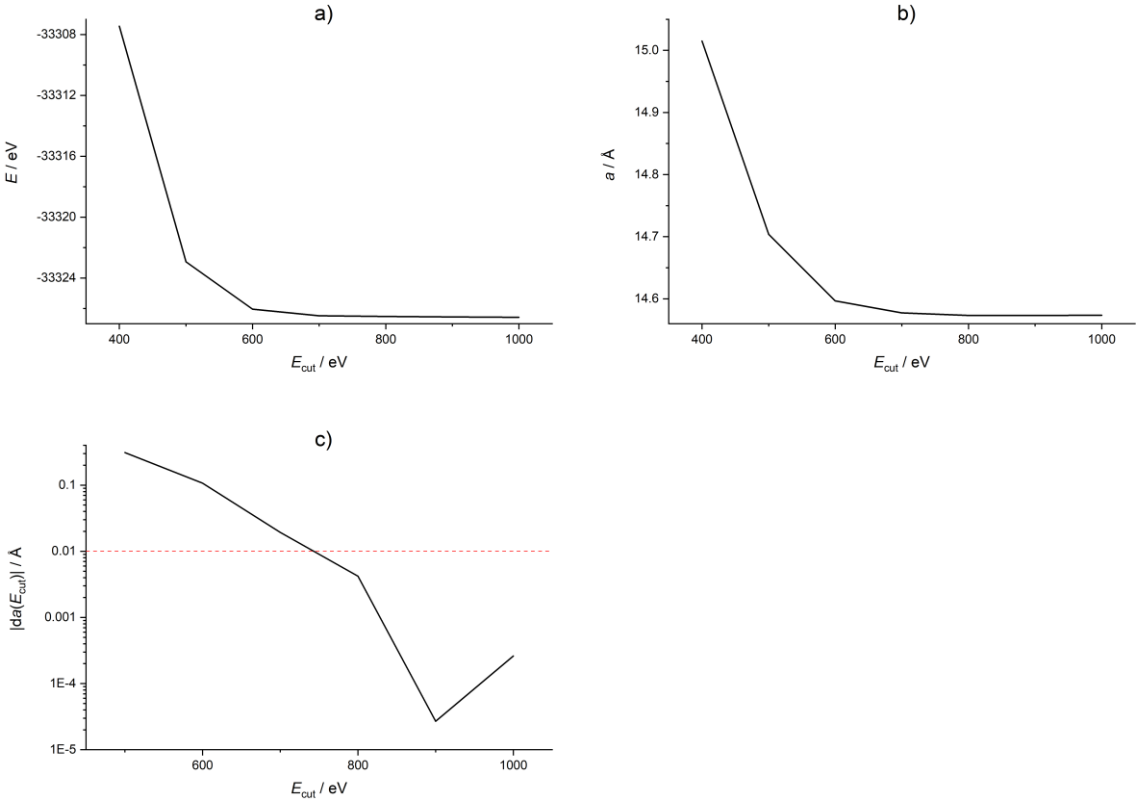

Figure S23. SOD-ZIF-71: Convergence of a) total energy, b) lattice parameter *a* and c) lattice parameter *a* (derivation).

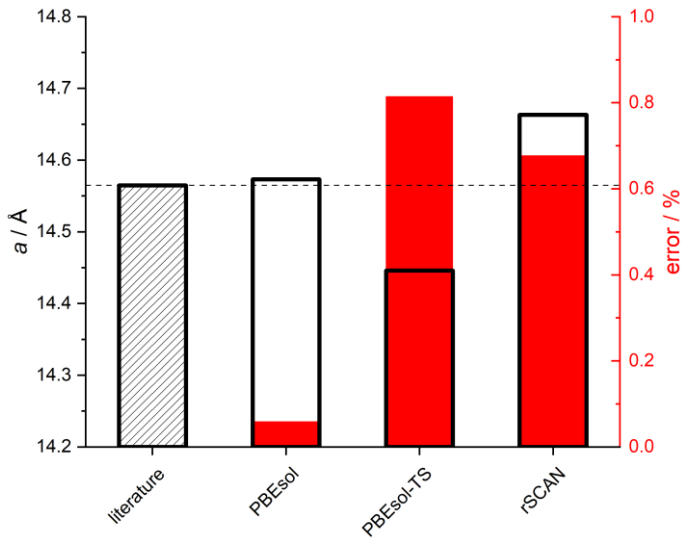

Figure S24. SOD-ZIF-71: XC functional benchmark (absolute value black with relative error in red). Literature value taken from Reference [9].

SALEM-2

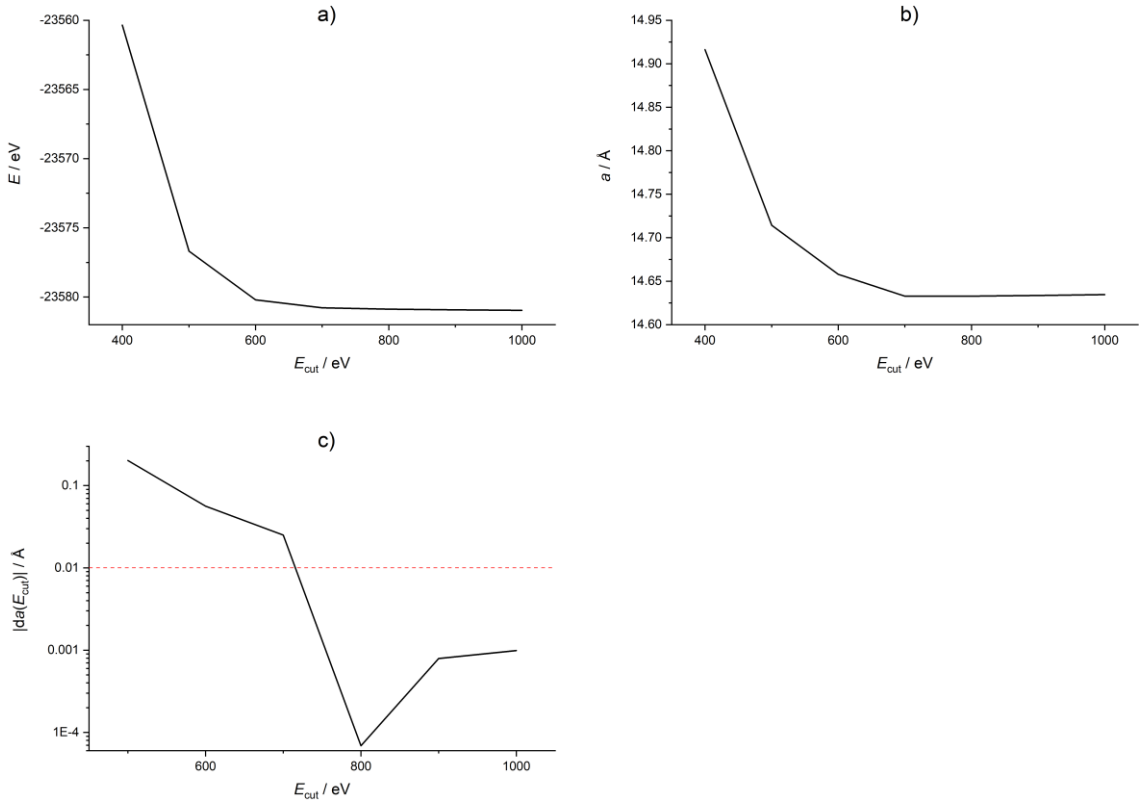

Figure S25. SALEM-2: Convergence of a) total energy, b) lattice parameter *a* and c) lattice parameter *a* (derivation).

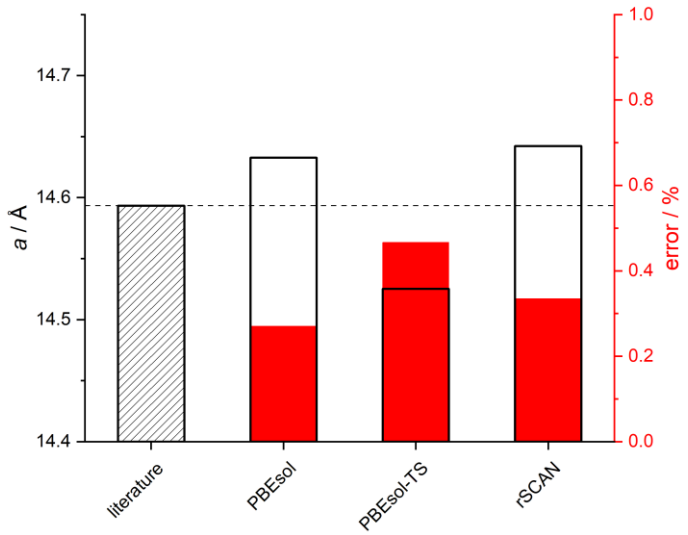

Figure S26. SALEM-2: XC functional benchmark (absolute value black with relative error in red). Literature value taken from Reference [10].

ZIF-1

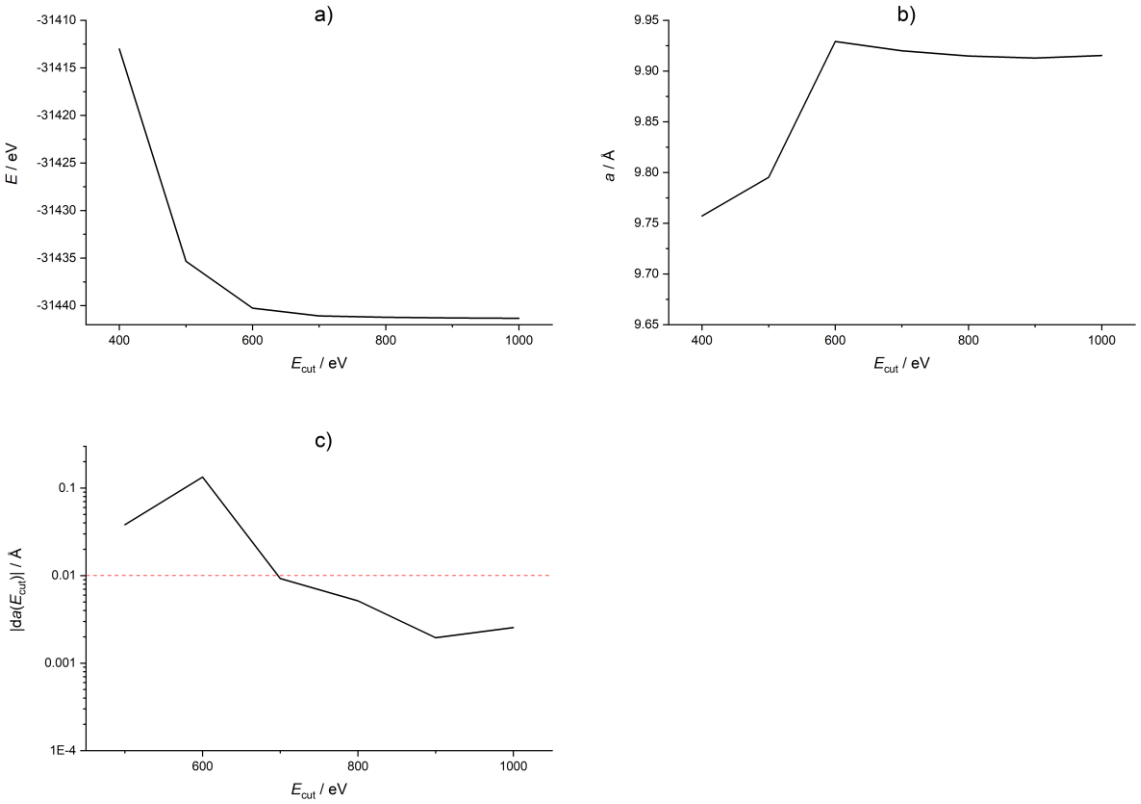

Figure S27. ZIF-1: Convergence of a) total energy, b) lattice parameter *a* and c) lattice parameter *a* (derivation).

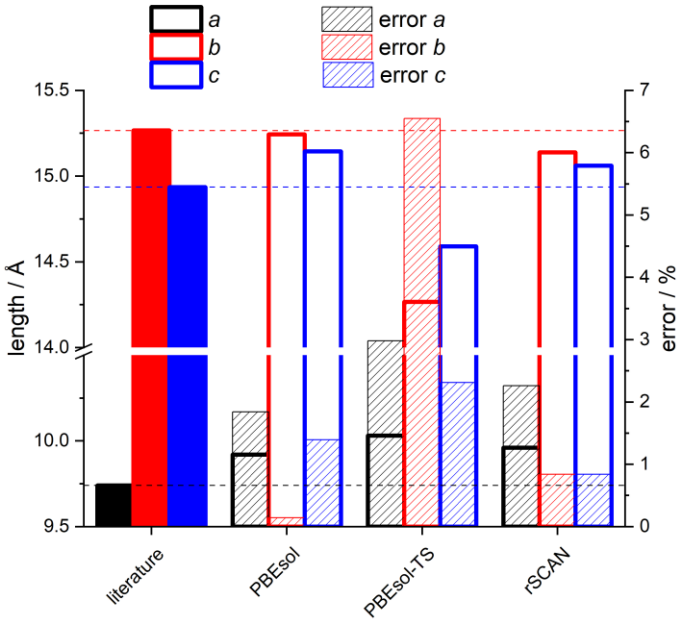

Figure S28. ZIF-1: XC functional benchmark with lattice parameters *a*, *b* and *c* (absolute values solid with relative errors hatched). Literature value taken from Reference [11].

ZIF-10

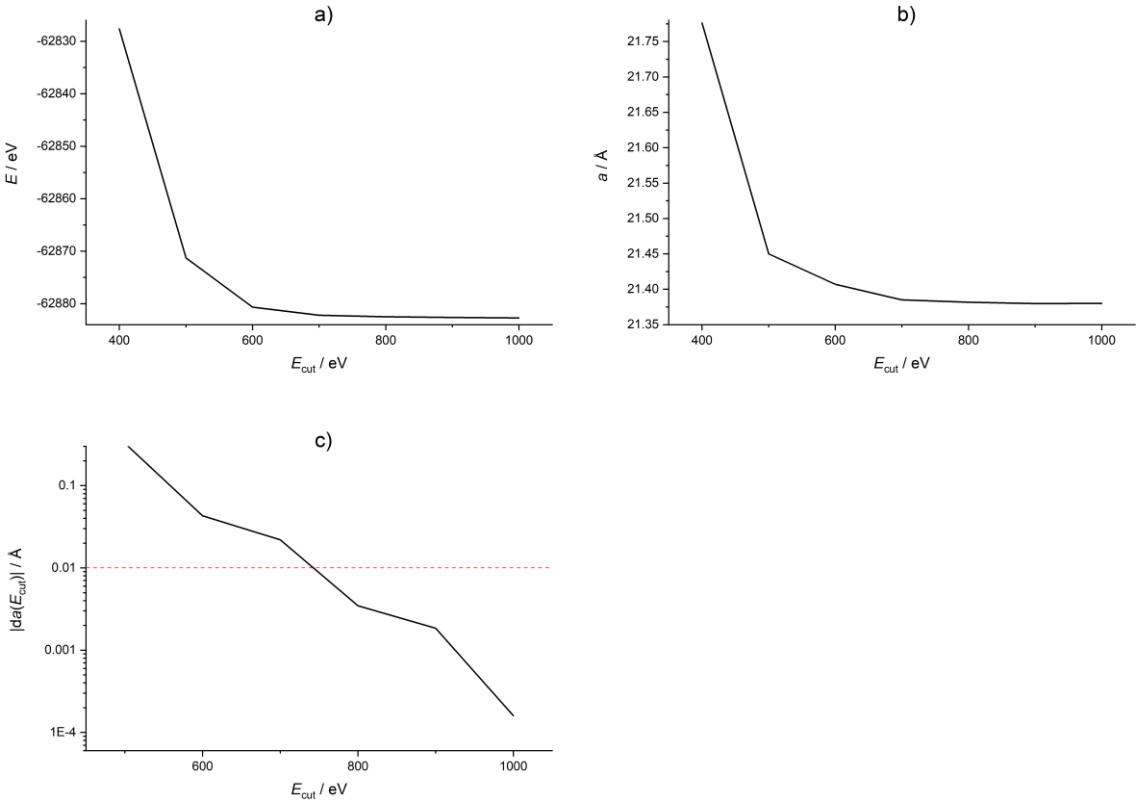

Figure S29. ZIF-10: Convergence of a) total energy, b) lattice parameter *a* and c) lattice parameter *a* (derivation).

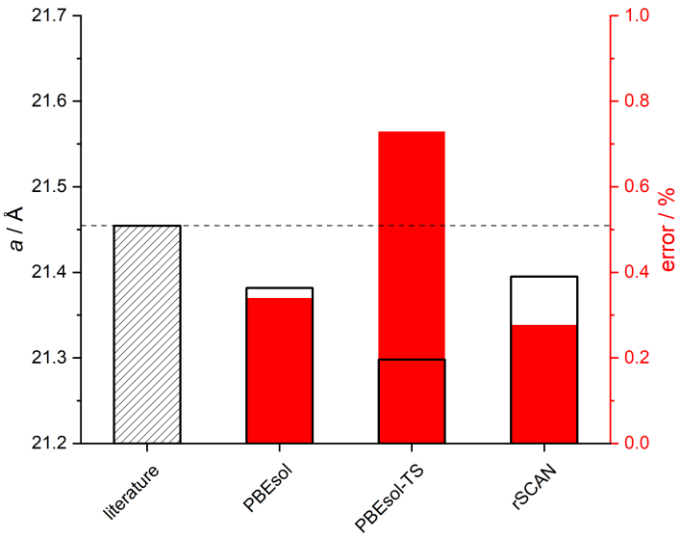

Figure S30. ZIF-10: XC functional benchmark (absolute value black with relative error in red). Literature value taken from Reference [11].

ZIF-64

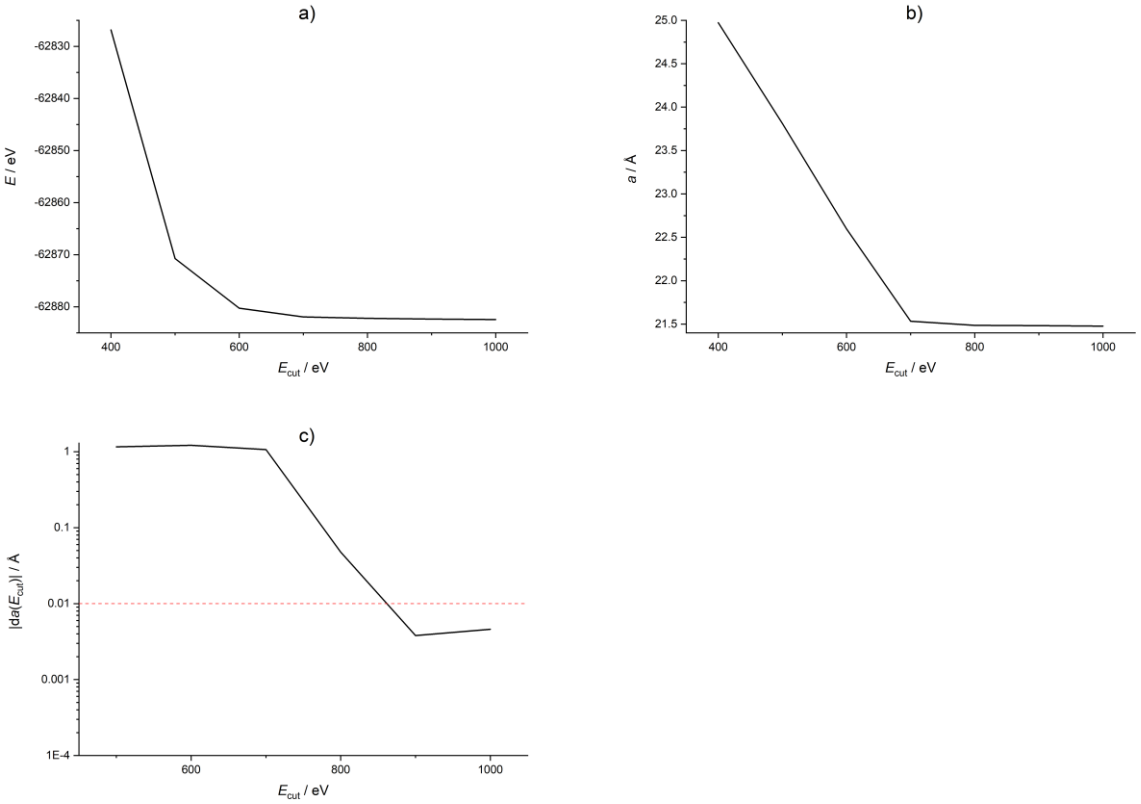

Figure S31. ZIF-64: Convergence of a) total energy, b) lattice parameter *a* and c) lattice parameter *a* (derivation).

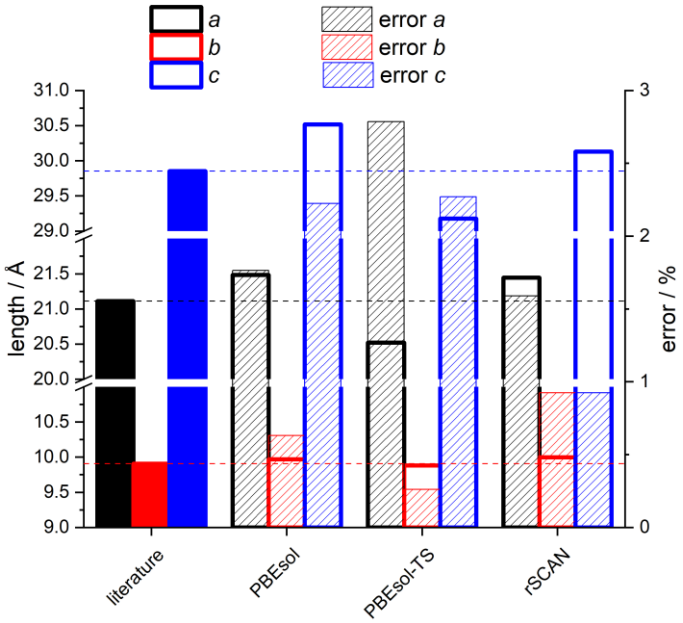

Figure S32. ZIF-64: XC functional benchmark with lattice parameters *a*, *b* and *c* (absolute values solid with relative errors hatched). Literature value taken from Reference [12].

ZIF-72

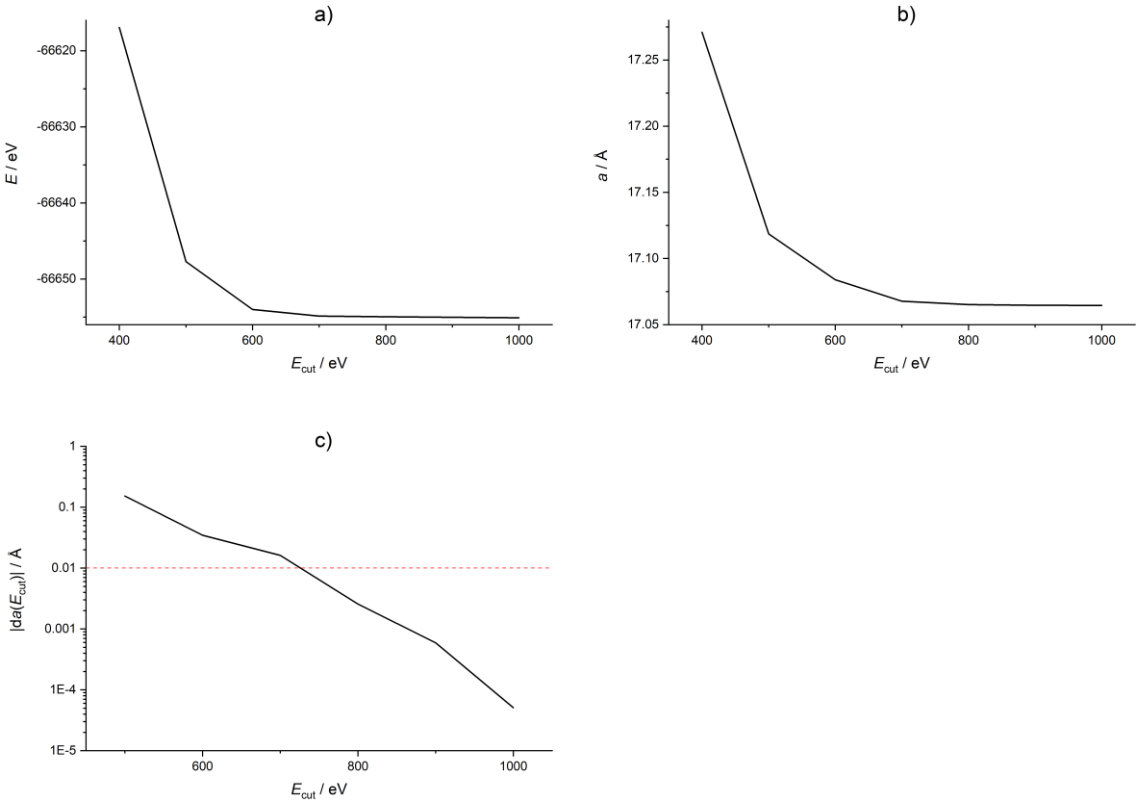

Figure S33. ZIF-72: Convergence of a) total energy, b) lattice parameter *a* and c) lattice parameter *a* (derivation).

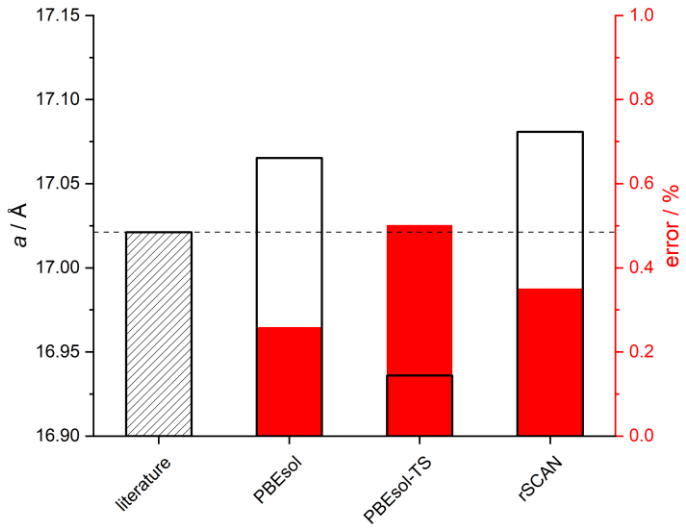

Figure S34. ZIF-72: XC functional benchmark (absolute value black with relative error in red). Literature value taken from Reference [12].

Al-MIL-53 (ht)

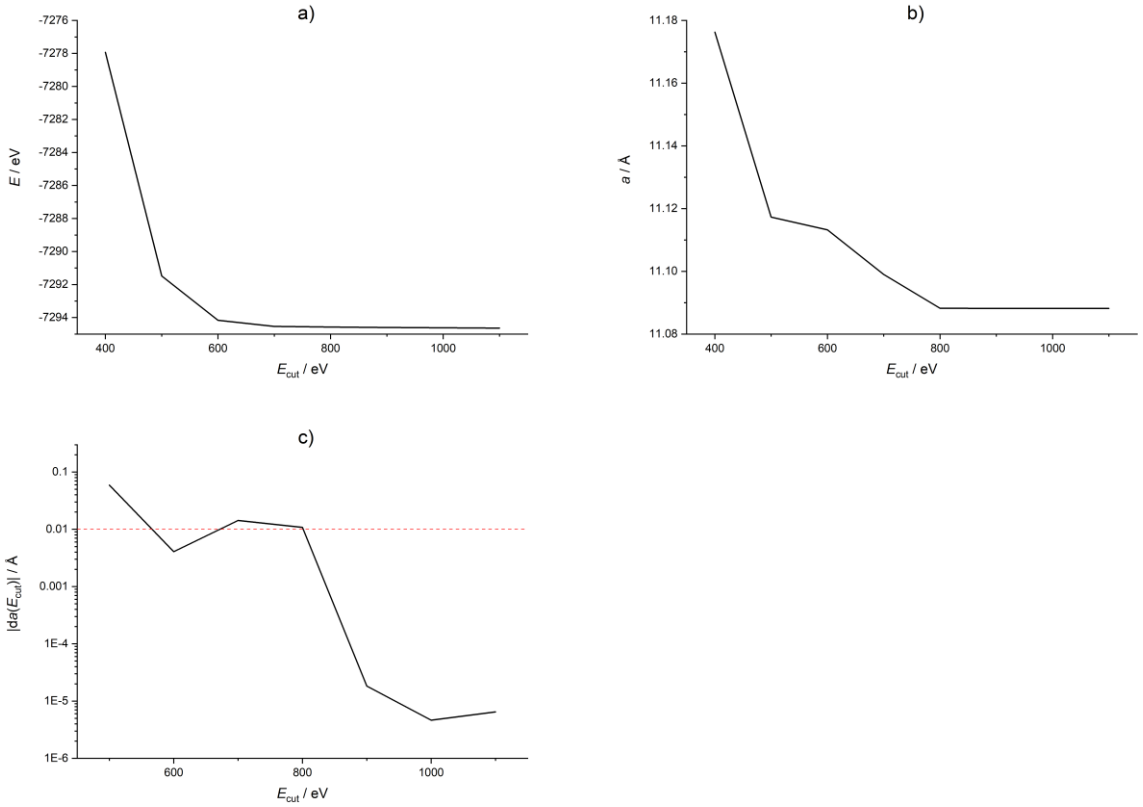

Figure S35. Al-MIL-53 (ht): Convergence of a) total energy, b) lattice parameter *a* and c) lattice parameter *a* (derivation).

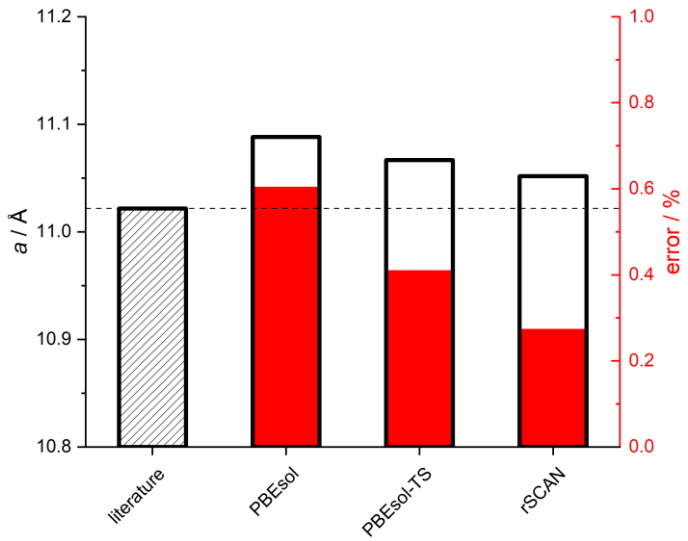

Figure S36. Al-MIL-53 (ht): XC functional benchmark (absolute value black with relative error in red). Literature value taken from Reference [13].

Section 2 Details of the periodic DFT models

Table S1. Details of the periodic DFT study and generated structural models of investigated Zr-based MOFs, ZIFs and Al-MIL-53: space group (SG), plane-wave kinetic energy cutoff (E_{cut}), sampling of Brillouin zone (BZ), exchange-correlation (XC) functional and lattice parameters of the primitive cells.

MOF	SG	E_{cut} / eV	BZ sampling	XC functional	*a* / Å	*b* / Å	*c* / Å
UiO-66-F_4	*F*-43*m*	800	*Γ*	PBEsol-TS	14.75	14.75	14.75
UiO-67	*F*-43*m*	800	*Γ*	rSCAN	19.02	19.02	19.02
Zr-*fum* MOF	*P*23	800	*Γ*	rSCAN	17.88	17.88	17.88
MIL-140A	*C*2/*c*	800	1×1×2	PBEsol-TS	13.41	13.41	7.81
MIL-140A-F	*P*1	800	1×1×2	PBEsol-TS	13.41	13.46	7.80
MIL-140A-Cl	*P*1	800	1×1×2	PBEsol-TS	13.40	13.49	7.79
MIL-140A-Br	*P*1	800	1×1×2	PBEsol-TS	13.39	13.49	7.80
MIL-140A-NO_2	*P*1	800	1×1×2	PBEsol-TS	13.35	13.47	7.81
ZIF-8	*Cm*	800	*Γ*	PBEsol-TS	14.57	14.57	14.57
ZIF-318	*Cm*	800	*Γ*	rSCAN	15.27	15.27	14.95
ZIF-90	*R*3	800	*Γ*	PBE-TS	14.97	14.97	14.97
SOD-ZIF-71	*I*-43*m*	800	*Γ*	PBEsol	14.57	14.57	14.57
SALEM-2	*I*-43*m*	800	*Γ*	PBEsol	14.63	14.63	14.63
ZIF-1	$P2_1/c$	700	*Γ*	PBEsol	9.92	15.24	15.14
ZIF-10	*I*4/*mmm*	800	*Γ*	rSCAN	21.40	21.40	21.40
ZIF-64	*P*2/*c*	900	*Γ*	rSCAN	21.45	10.00	30.13
ZIF-72	*Ia*-3*d*	800	*Γ*	PBEsol	17.07	17.07	17.07
Al-MIL-53 (ht)	*Imma*	900	2×1×2	rSCAN	11.05	11.05	11.05

Section 3 Details of the molecular DFT calculations

All calculations were performed with a 434 points Lebedev grid.

Table S2. Parameters of the SCF convergence tolerances.

Parameter		Value
Energy change	TolE	1.0×10^{-8} Eh
1-El. energy change		1.0×10^{-5} Eh
Orbital gradient	TolG	1.0×10^{-5}
Orbital rotation angle	TolX	1.0×10^{-5}
DIIS error	TolErr	1.0×10^{-7}

Table S3. Parameters of the geometry optimization convergence tolerances.

Parameter		Value
Update method		BGFS
Energy change	TolE	1.0×10^{-6} Eh
Max. gradient	TolMAXG	1.0×10^{-4} Eh/bohr
RMS gradient	TolRMSG	3.0×10^{-5} Eh/bohr
Max. displacement	TolMAXD	1.0×10^{-3} bohr
RMS displacement	TolRMSD	6.0×10^{-4} bohr

The CP-SCF calculations were performed using the Pople solver and a convergence tolerance of 1.0×10^{-8}.

Section 4 XC functional benchmark for fragment approach

In a first step three Zr-based MOFs (UiO-66, MIL-140A and Zr-*fum* MOF) were used to perform benchmark calculations in order to determine a suitable XC functional for the fragment approach. Therefore, 5 different XC functionals were assessed and the resulting RI values were compared with periodic HSE06 calculations. The detailed analysis of the results for each XC functional included in the benchmark are given below in Figure S37.

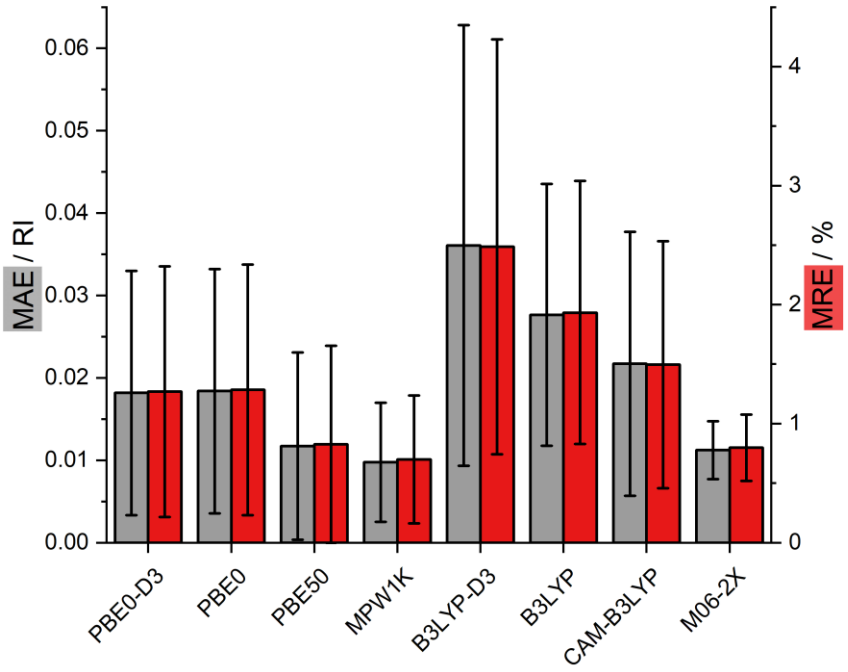

Figure S37. Fragment approach XC functional benchmark: mean absolute error (MAE) in grey and mean relative error (MRE) in red for the test set of three Zr-based MOFs.

Section 5 Polarizabilities of the MOF fragments

Table S4. MOF fragments and calculated polarizability volumes *α'* using the MPW1K functional.

Fragment		*α'* / Å^3
Al(III)		0.03963
Zn(II)		0.3114
Zr(IV)		0.4351
O(-II)		1.121
OH(-I)		1.751
mim(-I)	2-methyl-imidazolate	9.990
im(-I)	imidazolate	7.972
ica(-I)	imidazolate-2-carboxyaldehyde	10.81
dcim(-I)	4,5-dichloroimidazolate	11.55
cf$_3$im(-I)	2-trifluoromethyl-imidazolate	9.739
fum(-II)	fumarate	10.75
bdc(-II)		17.02
bdc-NO2(-II)	2-nitrobenzene-1,4-dicarboxylate	19.18
bdc-F(-II)	2-fluorobenzene-1,4-dicarboxylate	16.97
bdc-F4(-II)	2,3,5,6-tetrafluorobenzene-1,4-dicarboxylate	16.86
bdc-Cl(-II)	2-chlorobenzene-1,4-dicarboxylate	19.07
bdc-Br(-II)	2-bromorobenzene-1,4-dicarboxylate	20.12
bdc-I(-II)	2-iodorobenzene-1,4-dicarboxylate	22.43
bpdc(-II)	biphenyl-4,4'-dicarboxylate	29.10

Section 6 Fragment approach example calculation

The Lorenz-Lorentz equation relates RI and polarizability and can be expressed as:

$$n = \sqrt{\frac{1 + 2\frac{N\alpha}{3\varepsilon_0}}{1 - \frac{N\alpha}{3\varepsilon_0}}}$$

Using quantum chemical codes e.g. ORCA the polarizability volume *α'* can be calculated, which is related to the polarizability *α*:

$$\alpha' = \frac{\alpha}{4\pi\varepsilon_0}$$

Finally, the number density *N* can be derived from the unit cell volume *V*:

$$N = \frac{1}{V}$$

The following two examples demonstrate the use of the Lorenz-Lorentz equation to calculate the RI of MOFs using the polarizability of their respective fragments.

ZIF-8

ZIF-8 has 12 formula units per unit cell with a cell volume of 4784.86 Å^3.[6] The formula unit consists of one Zn(II) fragment and two *mim* fragments. The total polarizability volume adds up to:

$$\alpha'_{\text{ZIF-8}} = 12\left(\alpha'_{\text{Zn(II)}} + 2\alpha'_{mim}\right)$$

The RI of ZIF-8 results in:

$$n_{\text{ZIF-8}} = \sqrt{\frac{1 + 2\frac{\alpha'_{\text{ZIF-8}}4\pi}{3V_{\text{ZIF-8}}}}{1 - \frac{\alpha'_{\text{ZIF-8}}4\pi}{3V_{\text{ZIF-8}}}}} = 1.347$$

UiO-66

UiO-66 has four formula units per unit cell with a cell volume of 8929.65 Å^3.[3] The formula unit consists of six Zr(IV), four O(-II), four OH(-I) and six *bdc* fragments. The total polarizability volume adds up to:

$$\alpha'_{\text{UiO-66}} = 4\left(6\alpha'_{\text{Zr(IV)}} + 4\alpha'_{O(-II)} + 4\alpha'_{OH(-I)} + 6\alpha'_{bdc}\right)$$

The RI of UiO-66 results in:

$$n_{UiO-66} = \sqrt{\frac{1 + 2\frac{\alpha'_{UiO-66}4\pi}{3V_{UiO-66}}}{1 - \frac{\alpha'_{\text{ZIF-8}}4\pi}{3V_{UiO-66}}}} = 1.355$$

Section 7 Comparison of the calculation times

The periodic DFT calculations were performed with 80 cores while the fragment calculations were performed with 16 cores using Intel Cascade Lake Xeon Gold 6230N processors.

In the case of the UiO-66 MOF the total CPU time for the periodic DFT calculation is about 4117 hours and the fragment-based calculation takes about 23 CPU hours, which is more than 170 times faster.

Table S5. CPU times for UiO-66 fragments with MPW1K XC functional.

Fragment	t_{CPU} / s	t_{CPU} / h
O(-II)	704	
OH(-I)	2240	
Zr(IV)	832	
bdc(-II)	80432	
total	**84208**	**23.39**

Table S6. CPU times for periodic UiO-66 calculation with HSE06 XC functional.

Task	t_{CPU} / s	t_{CPU} / h
Ground state	8587840	
Optical properties	6234160	
total	**14822000**	**4117.22**

The calculations for ZIF-8 take about 3171 CPU hours for the periodic DFT and 5 CPU hours for the fragment-based approach, which is more than 620 times faster.

Table S7. CPU times for ZIF-8 fragments with MPW1K XC functional.

Fragment	t_{CPU} / s	t_{CPU} / h
Zn(II)	1040	
mim(-I)	17280	
total	**18320**	**5.09**

Table S8. CPU times for periodic ZIF-8 calculation with HSE06 XC functional.

Task	t_{CPU} / s	t_{CPU} / h
Ground state	4178560	
Optical properties	7238000	
total	**11416560**	**3171.27**

Finally, the calculations for Al-MIL-53 (ht) take approximately 1612 CPU hours for the periodic DFT and 23 CPU hours for the fragment-based approach, which is more than 70 times faster.

Table S9. CPU times for Al-MIL-53 (ht) fragments with MPW1K XC functional.

Fragment	t_{CPU} / s	t_{CPU} / h
OH(-I)	2240	
Al(III)	720	
bdc(-II)	80432	
total	**89440**	**22.96**

Table S10. CPU times for periodic Al-MIL-53 (ht) calculation with HSE06 XC functional.

Task	t_{CPU} / s	t_{CPU} / h
Ground state	1636293	
Optical properties	4166427	
total	**5802720**	**1611.87**

Section 8 Band structures

Table S11. Comparison of calculated band gaps.

MOF	E_g / eV
UiO-66-F_4	3.92
UiO-67	3.51
Zr-*fum* MOF	4.41
MIL-140A	4.04
MIL-140A-F	4.08
MIL-140A-Cl	3.72
MIL-140A-Br	3.56
MIL-140A-NO_2	4.10
ZIF-8	5.27
ZIF-318	5.31
ZIF-90	4.08
SOD-ZIF-71	5.03
SALEM-2	5.41
ZIF-1	5.28
ZIF-10	5.32
ZIF-64	5.36
ZIF-72	5.18
Al-MIL-53 (ht)	4.48

Zr-fum MOF

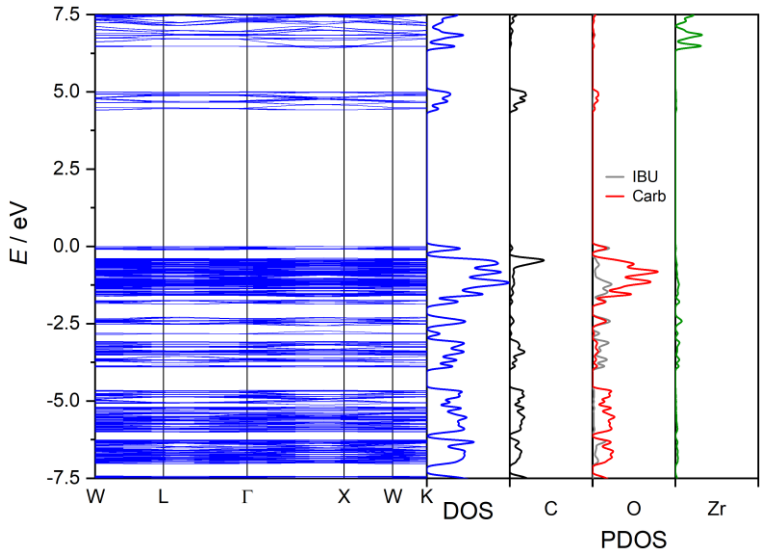

Figure S38. Zr-*fum* MOF band structure with DOS and PDOS.

UiO-66-F₄

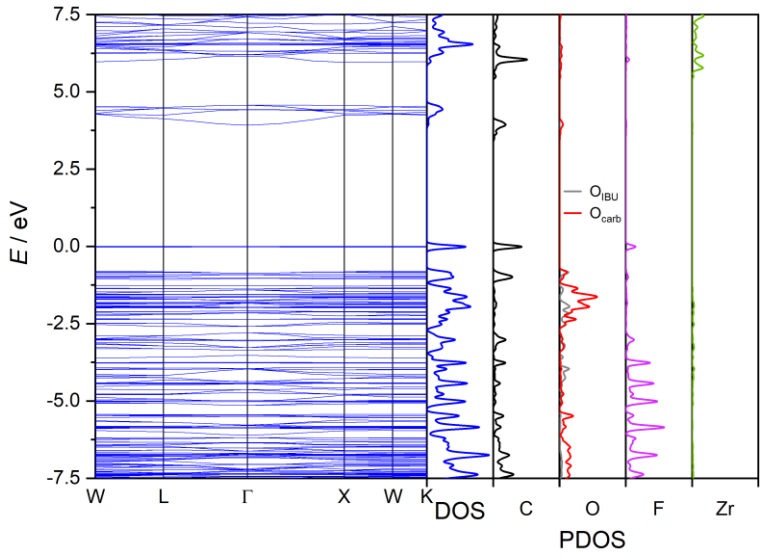

Figure S39. UiO-66-F₄ band structure with DOS and PDOS.

UiO-67

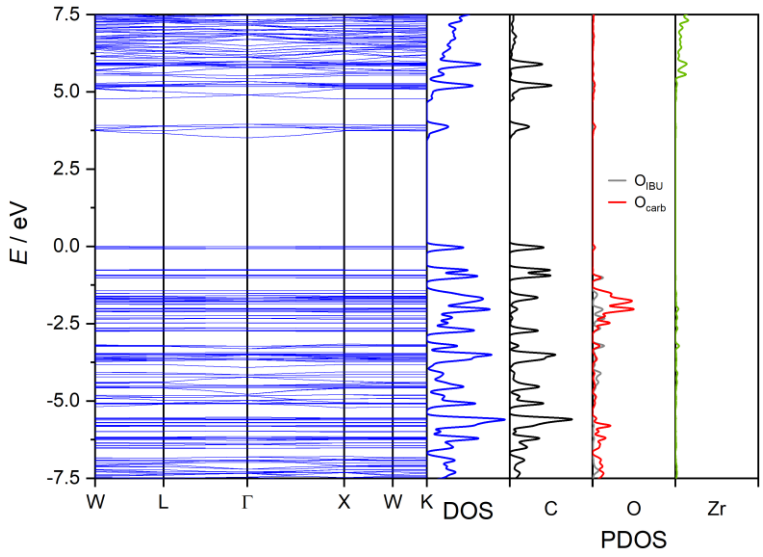

Figure S40. UiO-67 band structure with DOS and PDOS.

MIL-140A

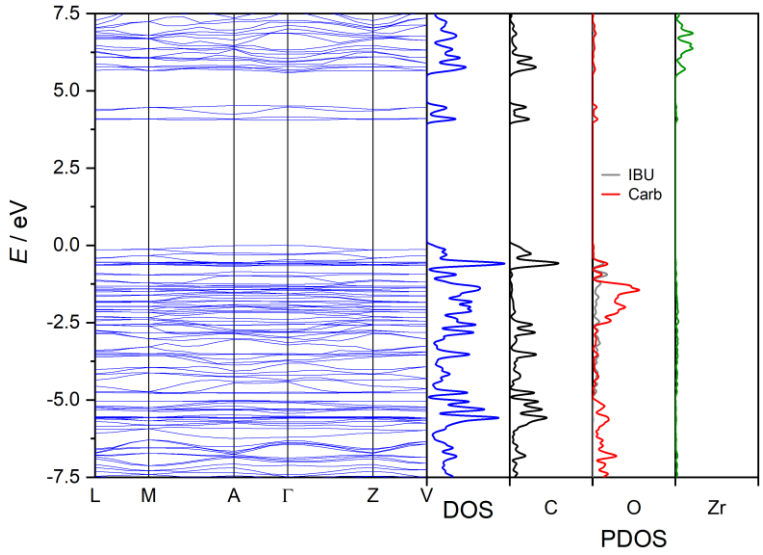

Figure S41. MIL-140A band structure with DOS and PDOS.

MIL-140A-F

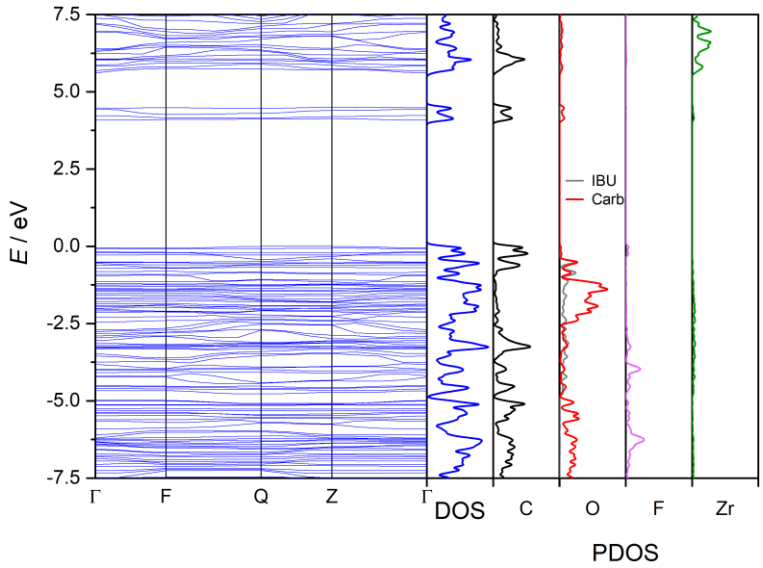

Figure S42. MIL-140A-F band structure with DOS and PDOS.

MIL-140A-Cl

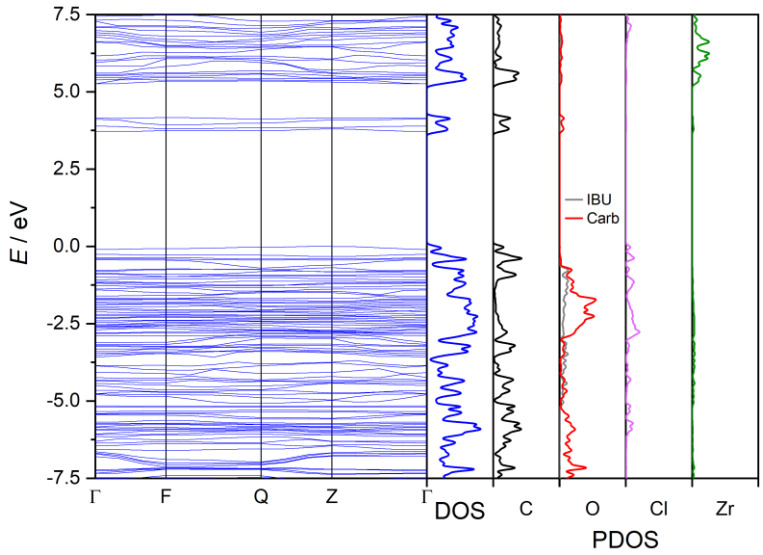

Figure S43. MIL-140A-Cl band structure with DOS and PDOS.

MIL-140A-Br

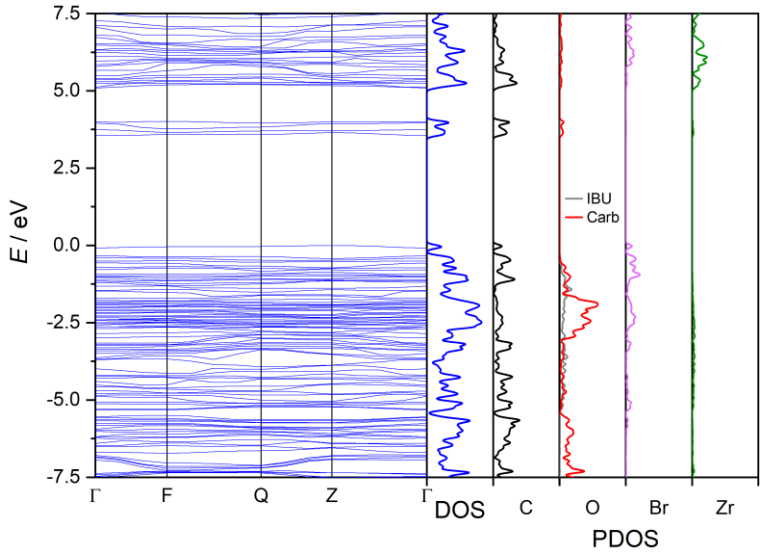

Figure S44. MIL-140A-Br band structure with DOS and PDOS.

MIL-140A-NO_2

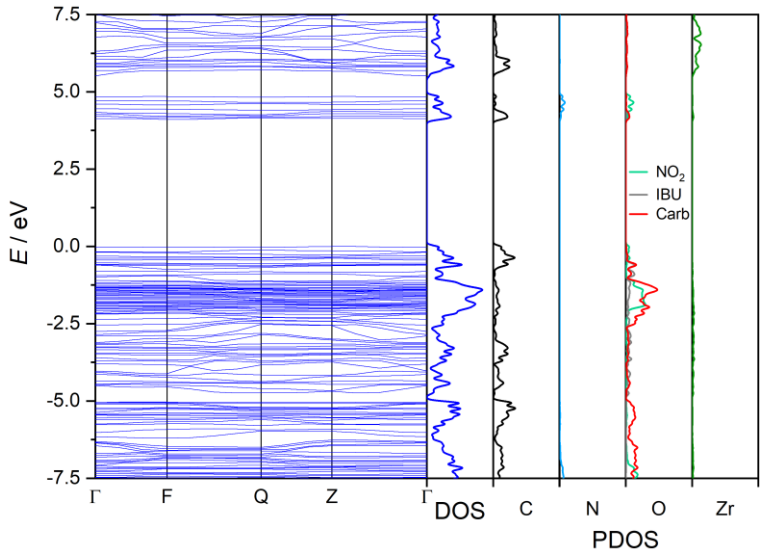

Figure S45. MIL-140A-NO_2 band structure with DOS and PDOS.

ZIF-8

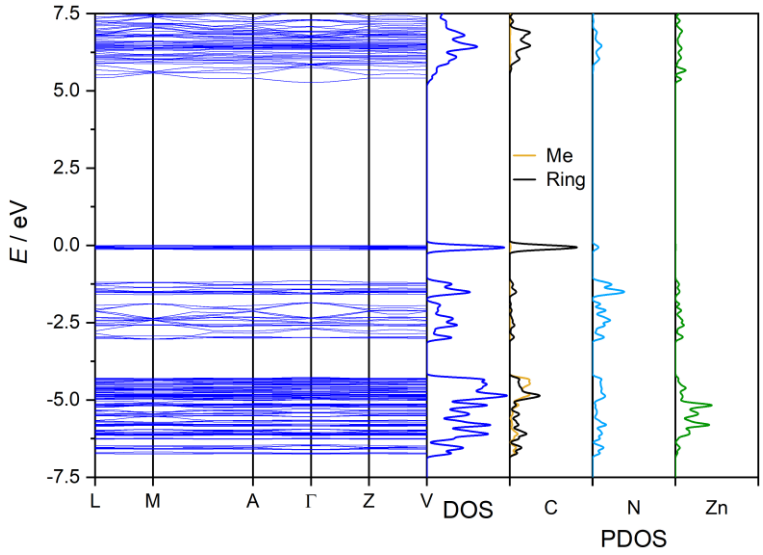

Figure S46. ZIF-8 band structure with DOS and PDOS.

ZIF-318

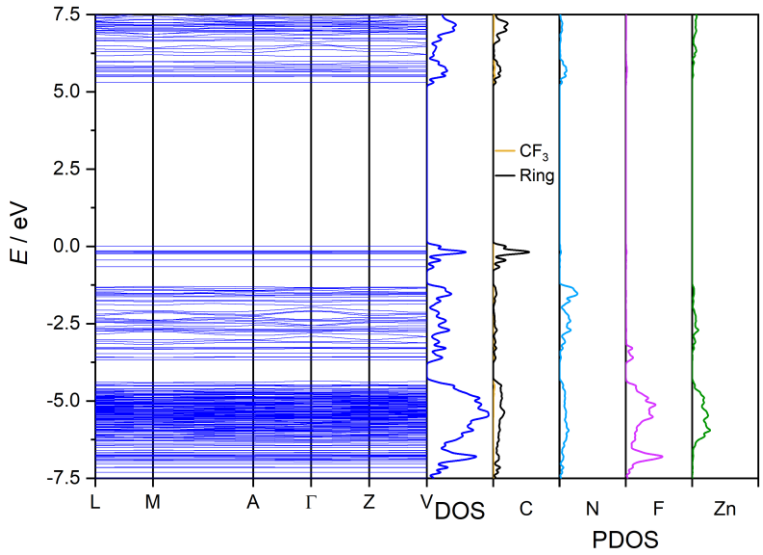

Figure S47. ZIF-318 band structure with DOS and PDOS.

ZIF-90

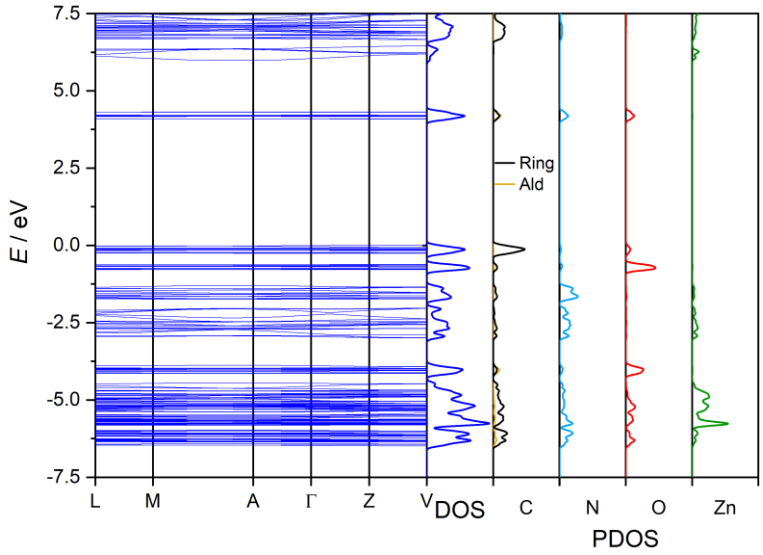

Figure S48. ZIF-90 band structure with DOS and PDOS.

SOD-ZIF-71

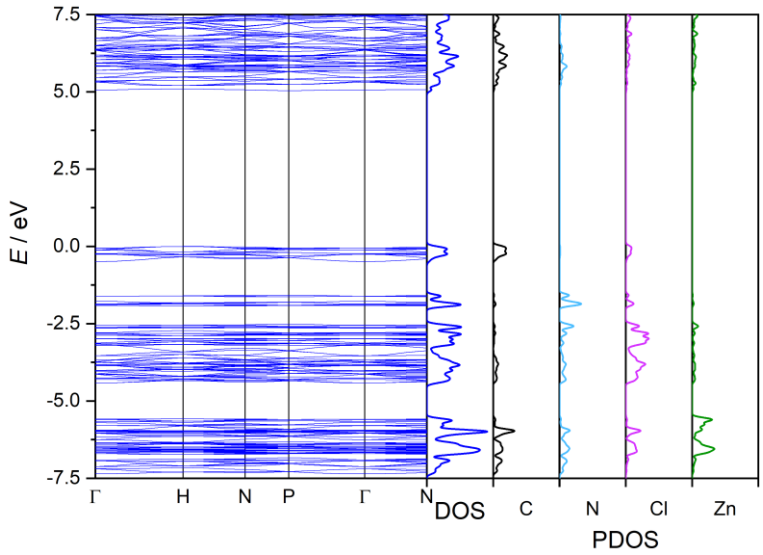

Figure S49. SOD-ZIF-71 band structure with DOS and PDOS.

SALEM-2

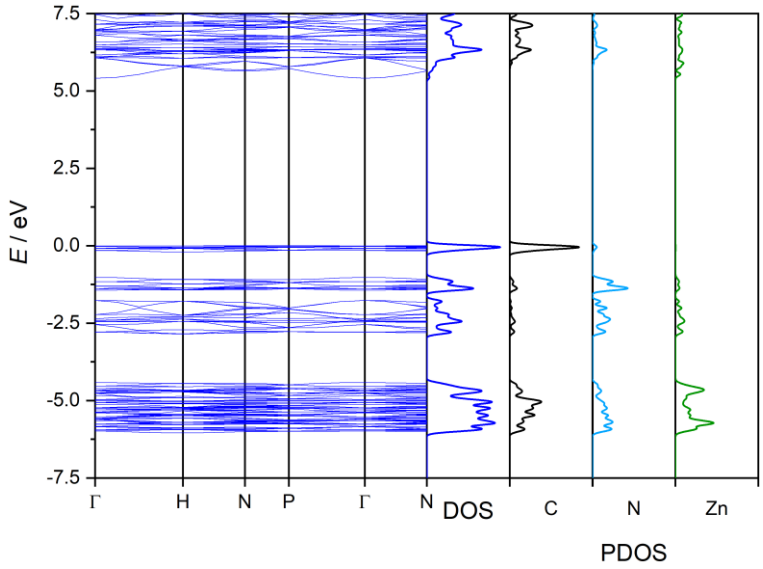

Figure S50. SALEM-2 band structure with DOS and PDOS.

ZIF-1

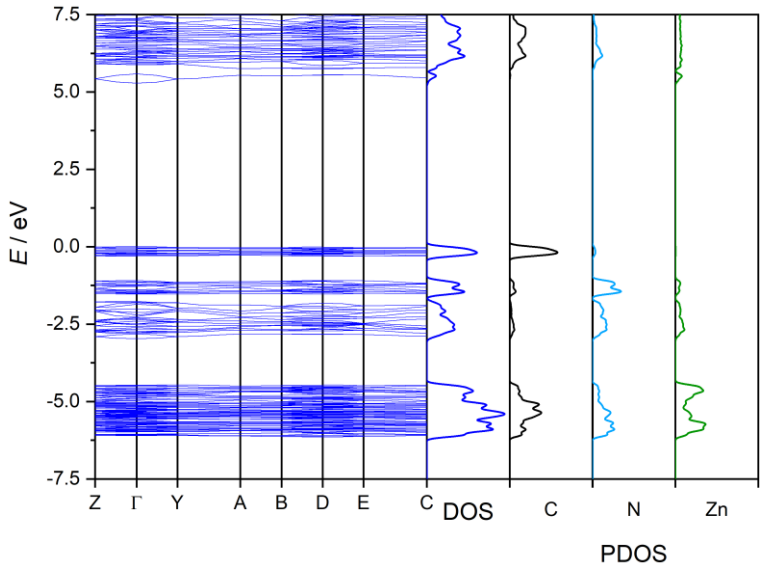

Figure S51. ZIF-1 band structure with DOS and PDOS.

ZIF-10

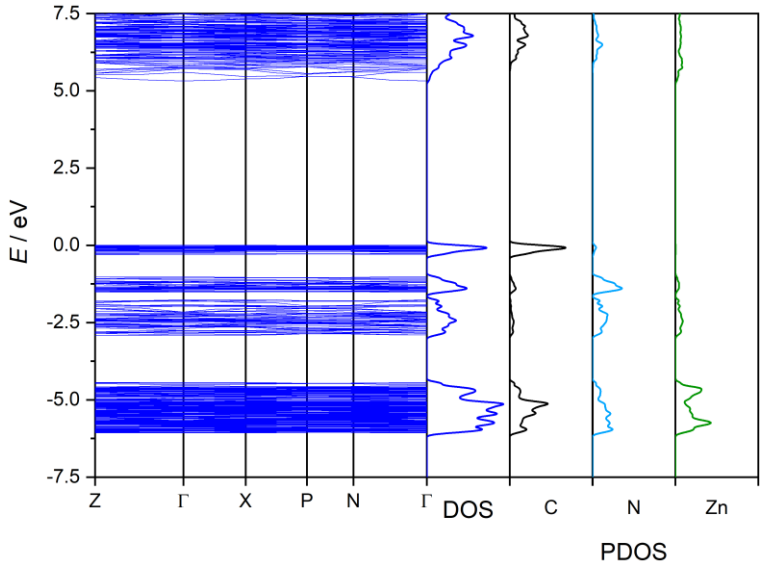

Figure S52. ZIF-10 band structure with DOS and PDOS.

ZIF-64

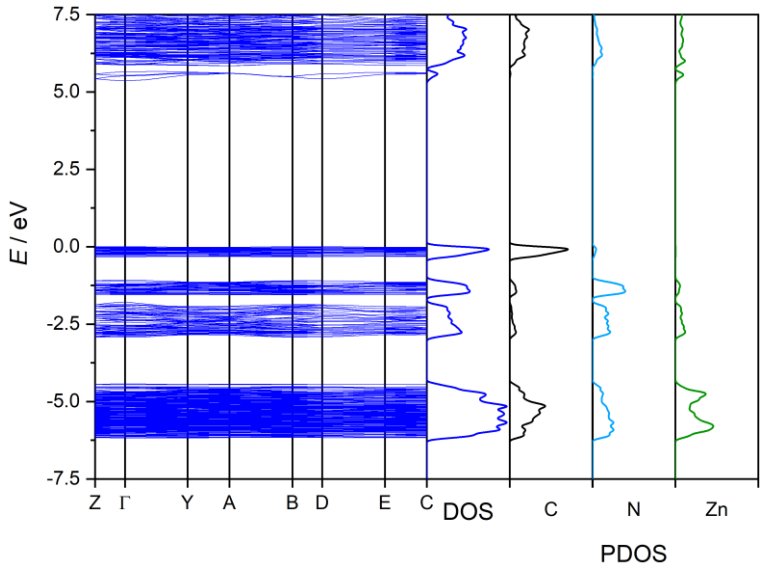

Figure S53. ZIF-64 band structure with DOS and PDOS.

ZIF-72

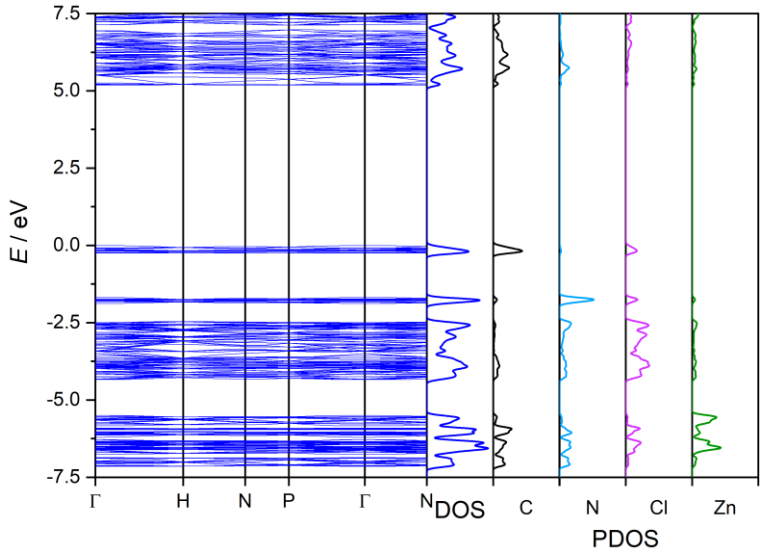

Figure S54. ZIF-72 band structure with DOS and PDOS.

Al-MIL-53 (ht)

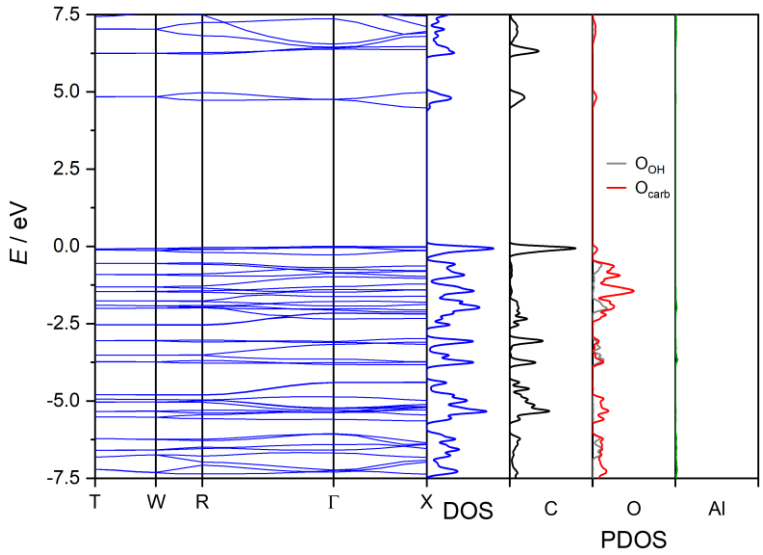

Figure S55. Al-MIL-53 (ht) band structure with DOS and PDOS.

Section 9 Dispersion of the refractive indices

UiO-66 type MOFs

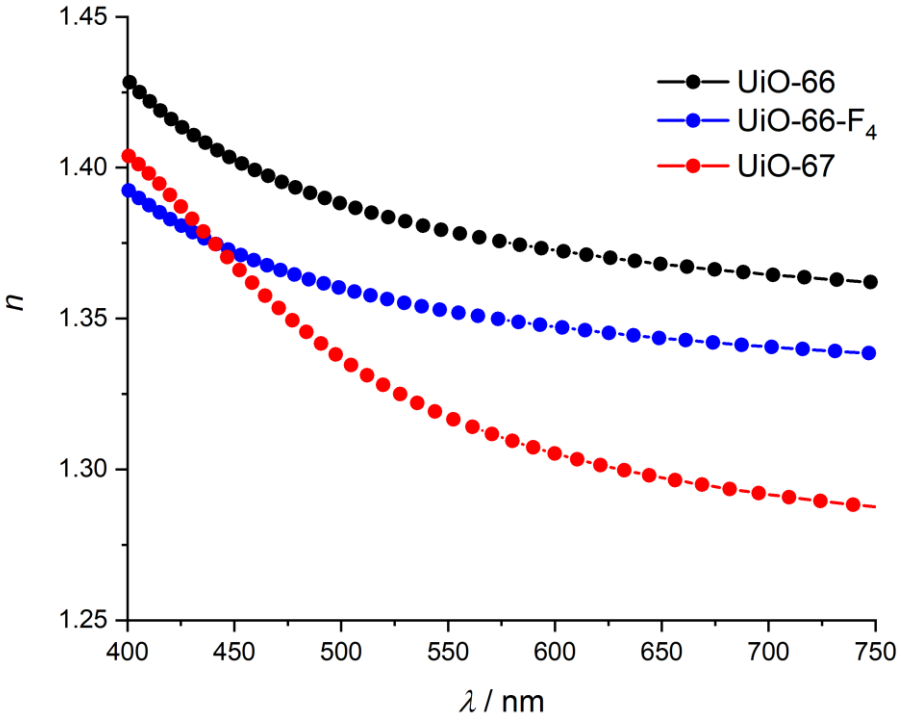

Figure S56. Refractive index dispersion of UiO-66-F_4 and UiO-67 in comparison with UiO-66 (value taken from Reference [1]).

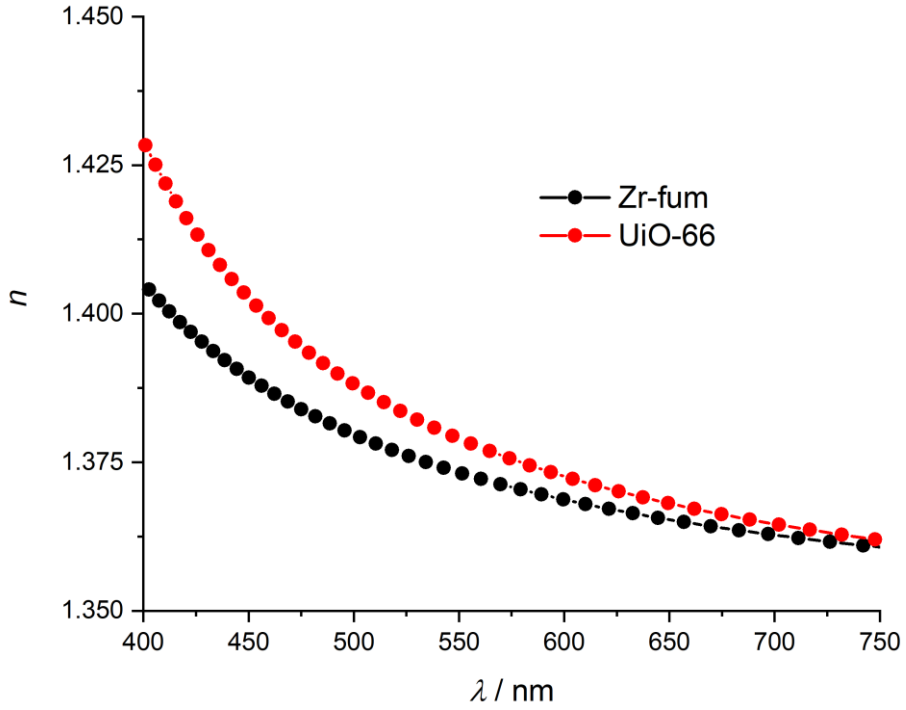

Figure S57. Refractive index dispersion of Zr-*fum* MOF in comparison with UiO-66 (value taken from Reference [1]).

MIL-140A and derivatives

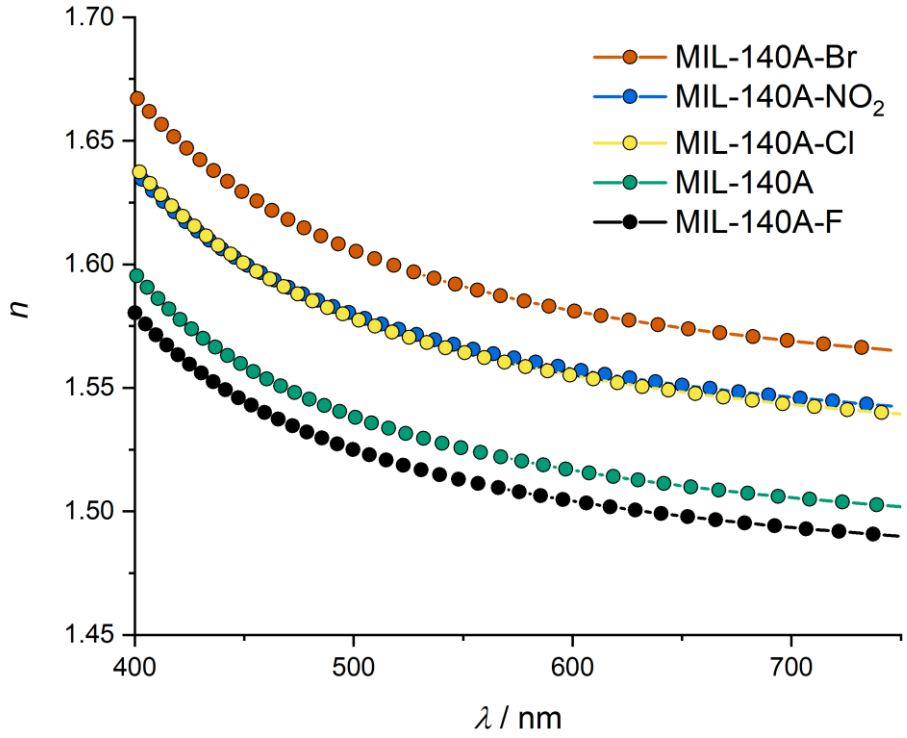

Figure S58. Refractive index dispersion of MIL-140A and its fluoro-, chloro-, bromo- and nitro derivatives.

ZIF-8 and derivatives

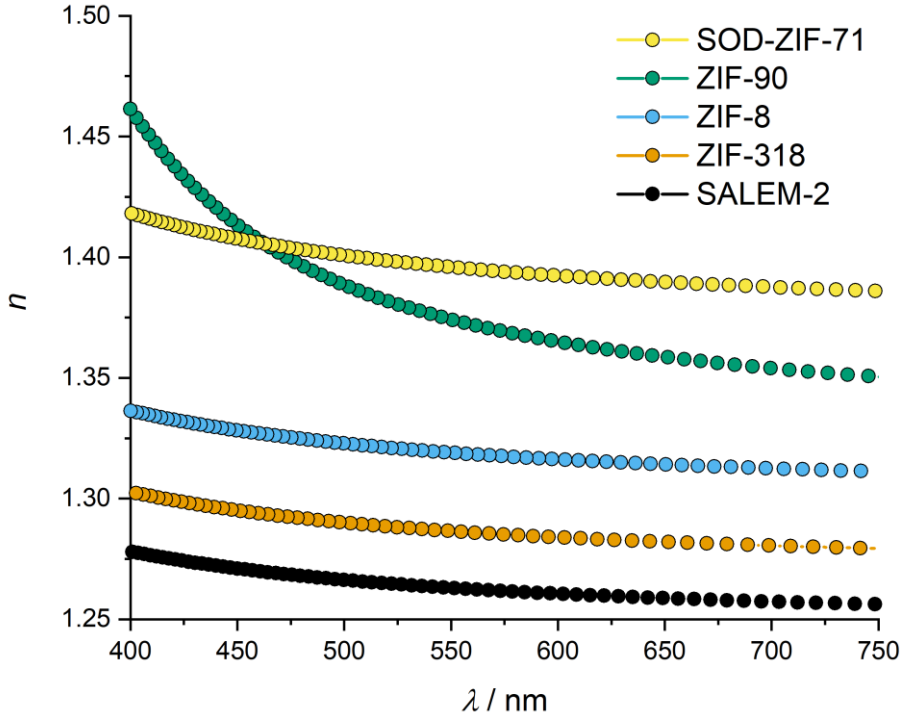

Figure S59. Refractive index dispersion of ZIF-8, ZIF-90, ZIF-318, SOD-ZIF-71 and SALEM-2.

ZIFs with im linker

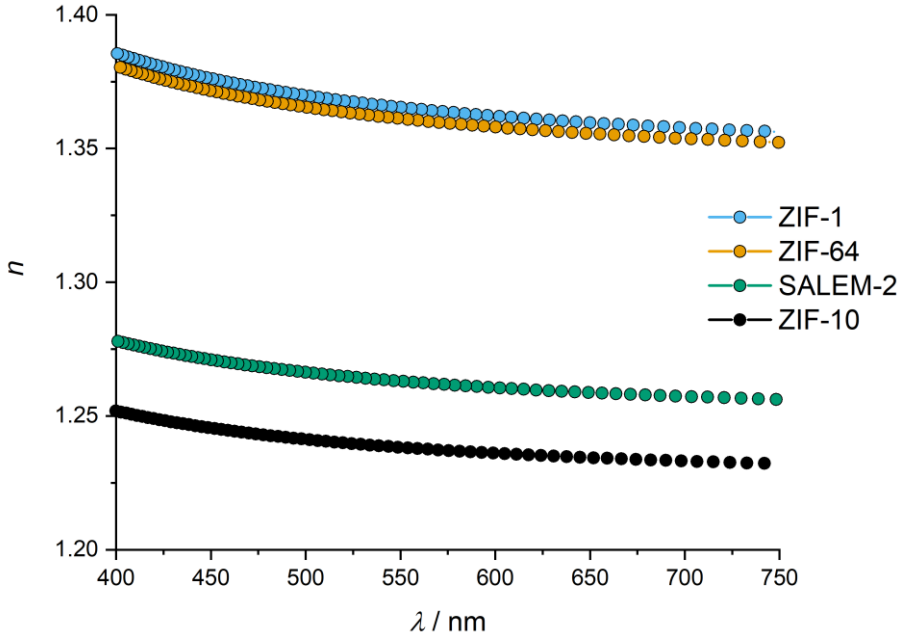

Figure S60. Refractive index dispersion of SALEM-2, ZIF-1, ZIF-10 and ZIF-64.

ZIF-72

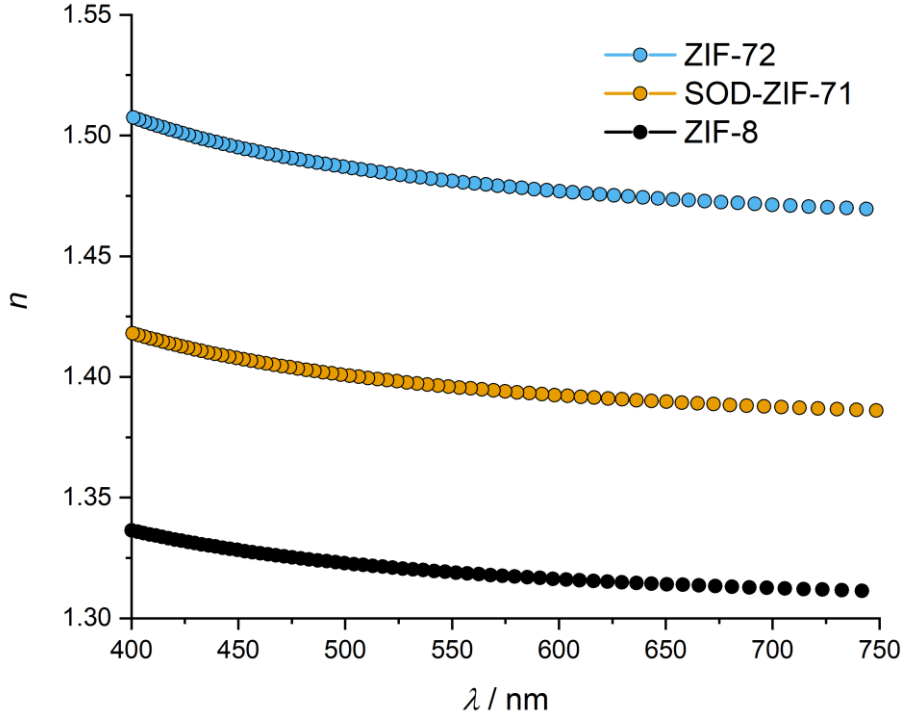

Figure S61. Refractive index dispersion of ZIF-72 in comparison with ZIF-8 and SOD-ZIF-71.

Al-MIL-53

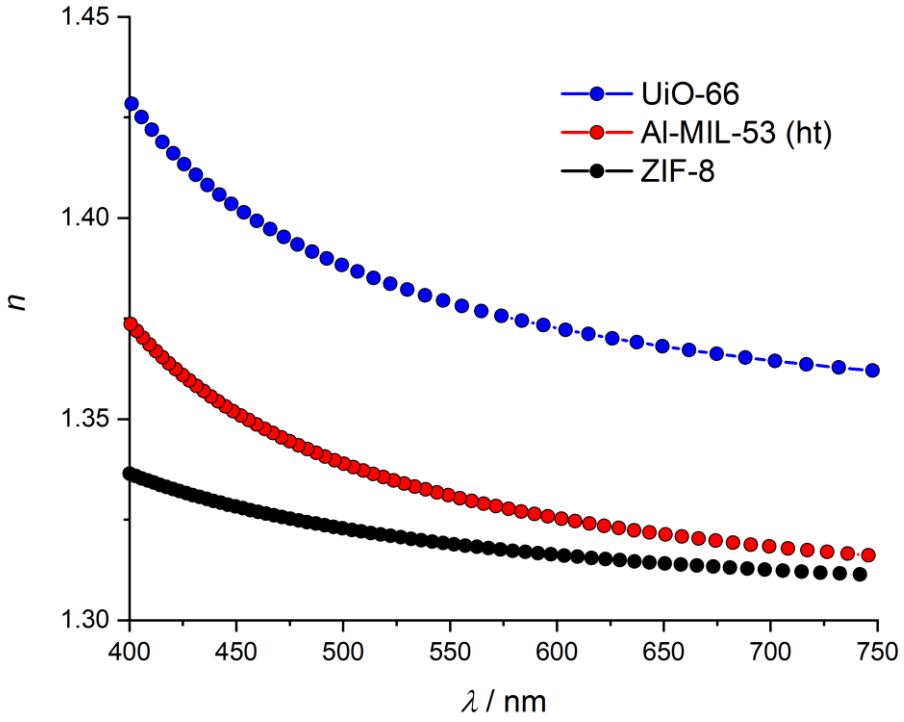

Figure S62. Refractive index dispersion of Al-MIL-53 (ht) in comparison with ZIF-8 and UiO-66 (value taken from Reference [1]).

Section 10 Comparison of the calculated refractive indices

Table S12. MOFs with the number of formula units per unit cell Z, the unit cell volume V, the refractive index at 589 nm calculated with periodic DFT $n_{periodic}$, the calculated static refractive index using the fragment approach $n_{fragment}$ and the relative error (RE) of $n_{fragment}$ compared with $n_{periodic}$.

MOF	Z	V / Å^3	$n_{periodic}$	$n_{fragment}$	RE / %
UiO-66	4	8929.65[3]	1.373	1.355	1.31
UiO-66-NO_2	4	8929.65	1.409	1.400	0.63
UiO-66-F	4	8929.65	1.375	1.354	1.54
UiO-66-F_4	4	8929.65	1.348	1.352	0.30
UiO-66-Cl	4	8929.65	1.416	1.398	1.32
UiO-66-Br	4	8929.65	1.433	1.420	0.90
UiO-66-I	4	8929.65	1.488	1.470	1.19
UiO-67	4	19423.68[3]	1.307	1.258	3.75
Zr-*fum* MOF	4	5713.39[4]	1.370	1.378	0.62
MIL-140A	8	2068.8[5]	1.519	1.514	0.33
MIL-140A-NO_2	8	2068.8	1.557	1.586	1.78
MIL-140A-F	8	2068.8	1.506	1.512	0.38
MIL-140A-Cl	8	2068.8	1.557	1.583	1.65
MIL-140A-Br	8	2068.8	1.583	1.620	2.31
ZIF-8	12	4784.86[6]	1.317	1.347	2.27
ZIF-318	12	4981.5[7]	1.284	1.323	2.96
ZIF-90	12	5152.2[8]	1.366	1.348	1.36
SOD-ZIF-71	12	4756.8[9]	1.393	1.410	1.20
SALEM-2	12	4767.33[10]	1.261	1.273	0.97
ZIF-1	8	2195.8[11]	1.363	1.411	3.54
ZIF-10	32	14210.8[11]	1.237	1.242	0.47
ZIF-64	16	4414.6[12]	1.359	1.408	3.67
ZIF-72	24	7592.41[12]	1.478	1.493	1.00
Al-MIL-53 (ht)	4	1411.9[13]	1.326	1.365	2.88

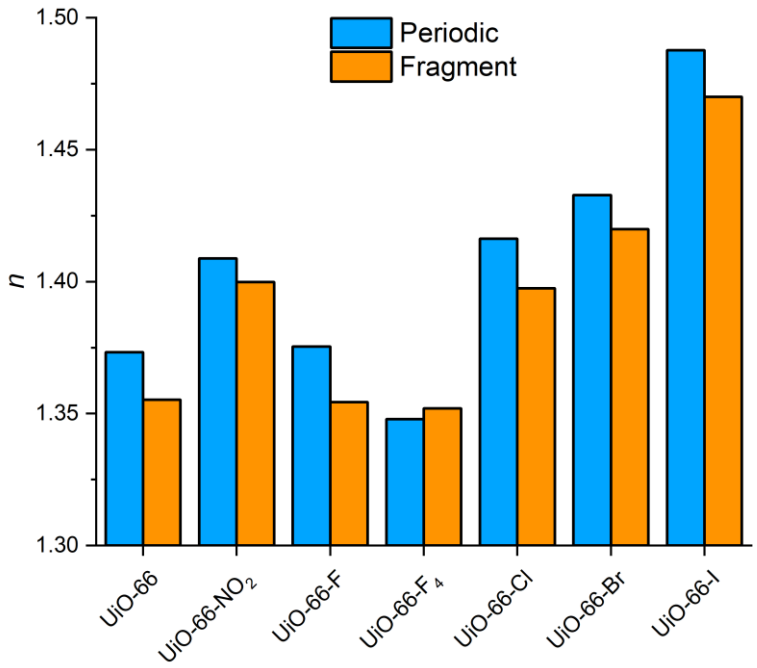

Figure S63. RI of UiO-66 type MOFs calculated with periodic DFT and fragment approach.

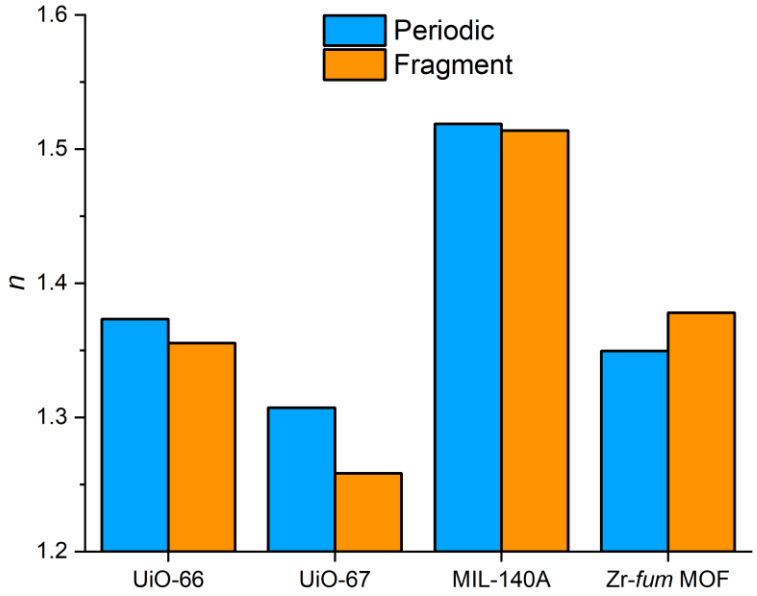

Figure S64. RI of MOFs with UiO-topology (UiO-66, UiO-67 and Zr-*fum* MOF) and MIL-140A calculated with periodic DFT and fragment approach.

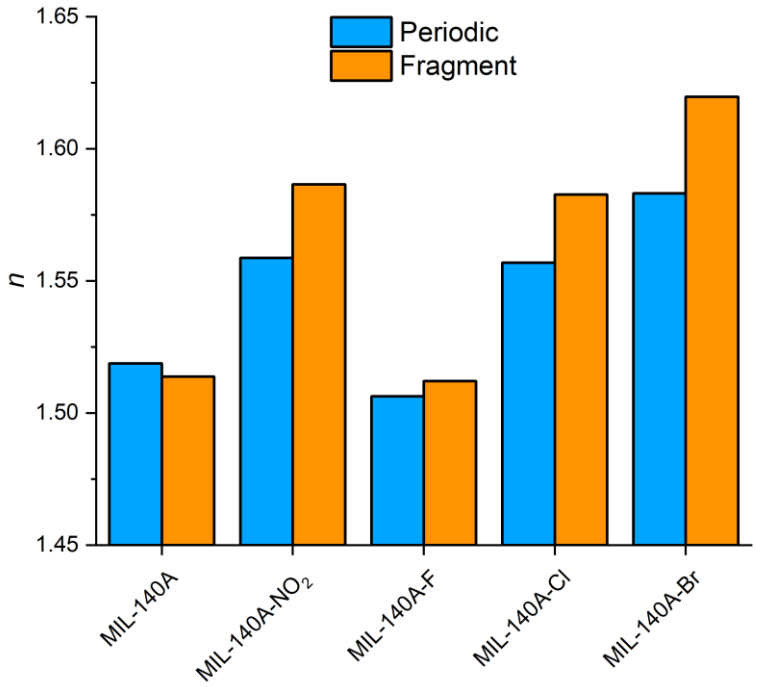

Figure S65. RI of MIL-140A type MOFs calculated with periodic DFT and fragment approach.

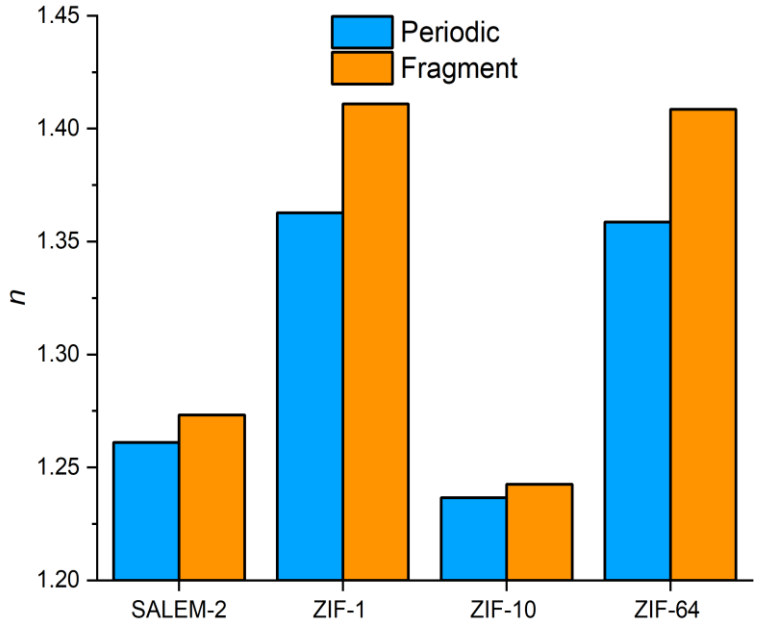

Figure S66. RI of ZIFs based on *mim* linker calculated with periodic DFT and fragment approach.

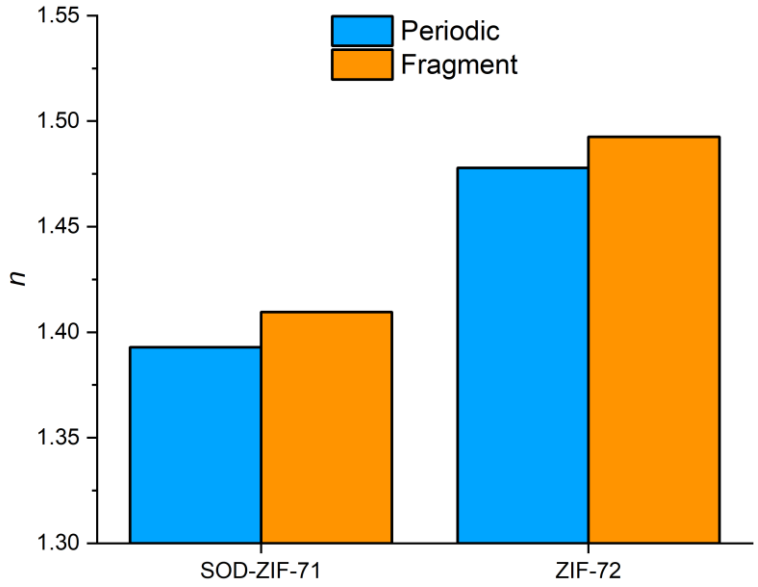

Figure S67. RI of ZIFs based on the *dcim* linker calculated with periodic DFT and fragment approach.

References

[1] M. Treger, A. Hannebauer, A. Schaate, J. L. Budde, P. Behrens, A. M. Schneider, *Phys. Chem. Chem. Phys.* **2023**, *25*, 6333.

[2] M. Treger, A. Hannebauer, P. Behrens, A. M. M. Schneider, *Phys. Chem. Chem. Phys.* **2023**,DOI: 10.1039/D3CP01291C.

[3] S. Øien, D. Wragg, H. Reinsch, S. Svelle, S. Bordiga, C. Lamberti, K. P. Lillerud, *Cryst. Growth Des.* **2014**, *14*, 5370.

[4] G. Wißmann, A. Schaate, S. Lilienthal, I. Bremer, A. M. Schneider, P. Behrens, *Microporous Mesoporous Mat.* **2012**, *152*, 64.

[5] V. Guillerm, F. Ragon, M. Dan-Hardi, T. Devic, M. Vishnuvarthan, B. Campo, A. Vimont, G. Clet, Q. Yang, G. Maurin et al., *Angew. Chem.* **2012**, *124*, 9401.

[6] W. Morris, C. J. Stevens, R. E. Taylor, C. Dybowski, O. M. Yaghi, M. A. Garcia-Garibay, *J. Phys. Chem. C* **2012**, *116*, 13307.

[7] S. S. Mondal, M. Hovestadt, S. Dey, C. Paula, S. Glomb, A. Kelling, U. Schilde, C. Janiak, M. Hartmann, H.-J. Holdt, *CrystEngComm* **2017**, *19*, 5882.

[8] W. Morris, C. J. Doonan, H. Furukawa, R. Banerjee, O. M. Yaghi, *J. Am. Chem. Soc.* **2008**, *130*, 12626.

[9] M. E. Schweinefuss, S. Springer, I. A. Baburin, T. Hikov, K. Huber, S. Leoni, M. Wiebcke, *Dalton Trans.* **2014**, *43*, 3528.

[10] O. Karagiaridi, M. B. Lalonde, W. Bury, A. A. Sarjeant, O. K. Farha, J. T. Hupp, *J. Am. Chem. Soc.* **2012**, *134*, 18790.

[11] K. S. Park, Z. Ni, A. P. Côté, J. Y. Choi, R. Huang, F. J. Uribe-Romo, H. K. Chae, M. O'Keeffe, O. M. Yaghi, *Proc. Natl. Acad. Sci. USA* **2006**, *103*, 10186.

[12] R. Banerjee, A. Phan, B. Wang, C. Knobler, H. Furukawa, M. O'Keeffe, O. M. Yaghi, *Science* **2008**, *319*, 939.

[13] T. Loiseau, C. Serre, C. Huguenard, G. Fink, F. Taulelle, M. Henry, T. Bataille, G. Férey, *Chemistry* **2004**, *10*, 1373.